

SBS Program Overview and GEP Experiment

Andrew Puckett

UConn

Hall A Winter Collaboration Meeting 2020

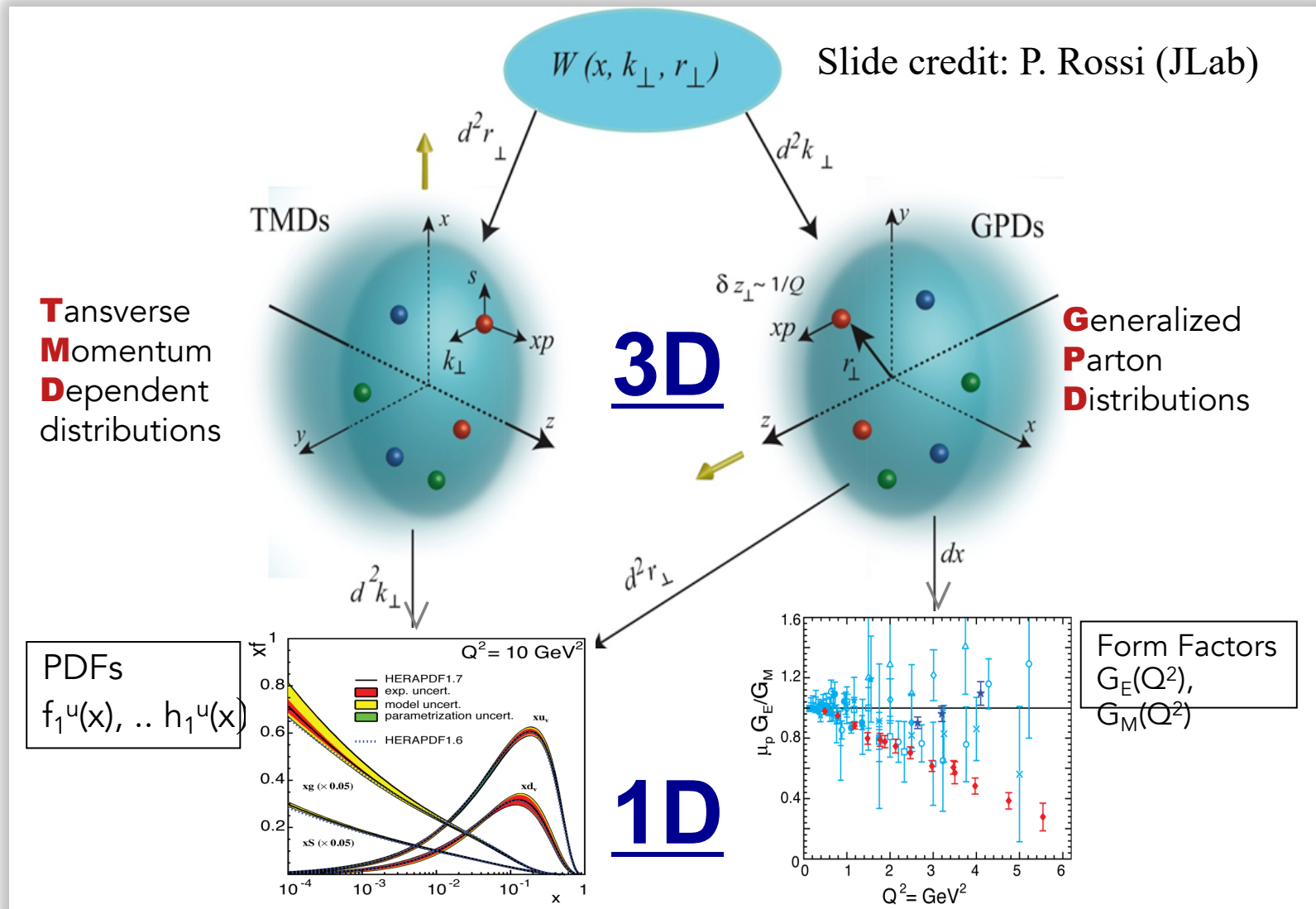
January 31, 2020

Acknowledgements

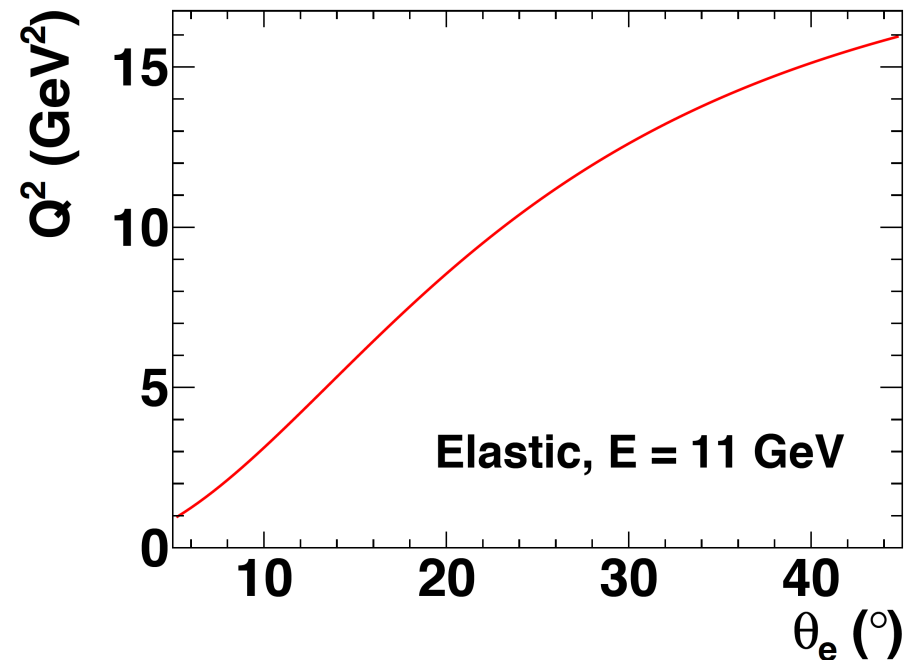
This work is supported by:

- SBS and Hall A collaborations
- Support from US Department Of Energy, Office of Science, Office of Nuclear Physics, Award ID DE-SC0014230 (Early Career research program)
- The University of Connecticut and Jefferson Lab

Tomography of the nucleon—OR: why we study high- Q^2 electron scattering



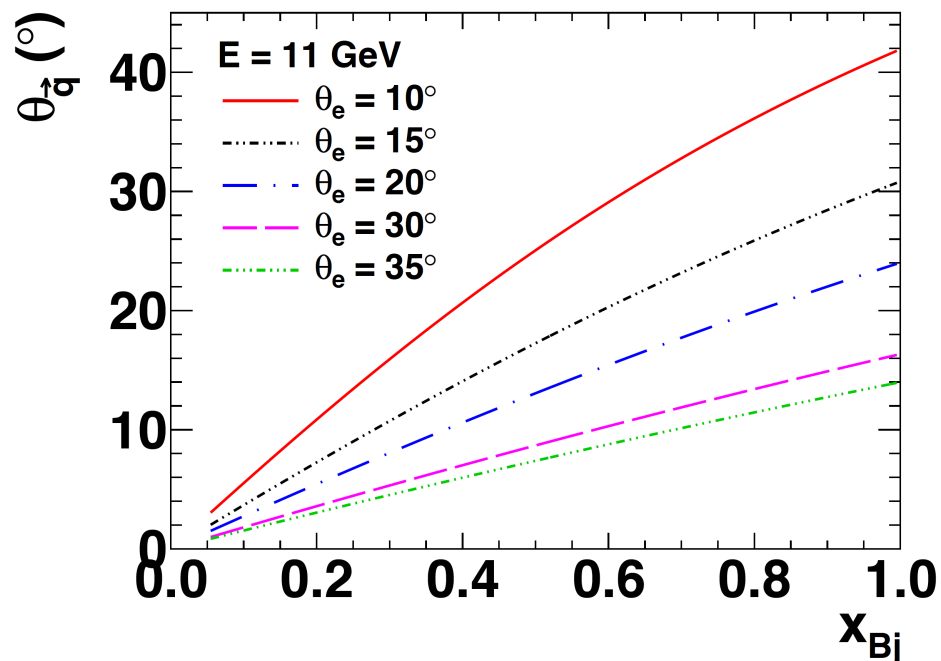
Electron Scattering Kinematics @11 GeV



- Measurements of elastic FFs, SIDIS, DVCS, etc., involve coincidence $N(e, e'X)$ (electroproduction) reactions, where $X =$
 - N' (elastic or quasi-elastic)
 - h (SIDIS or DVMP)
 - γ (DVCS)
- Virtual photon angle decreases as “inelasticity” increases:

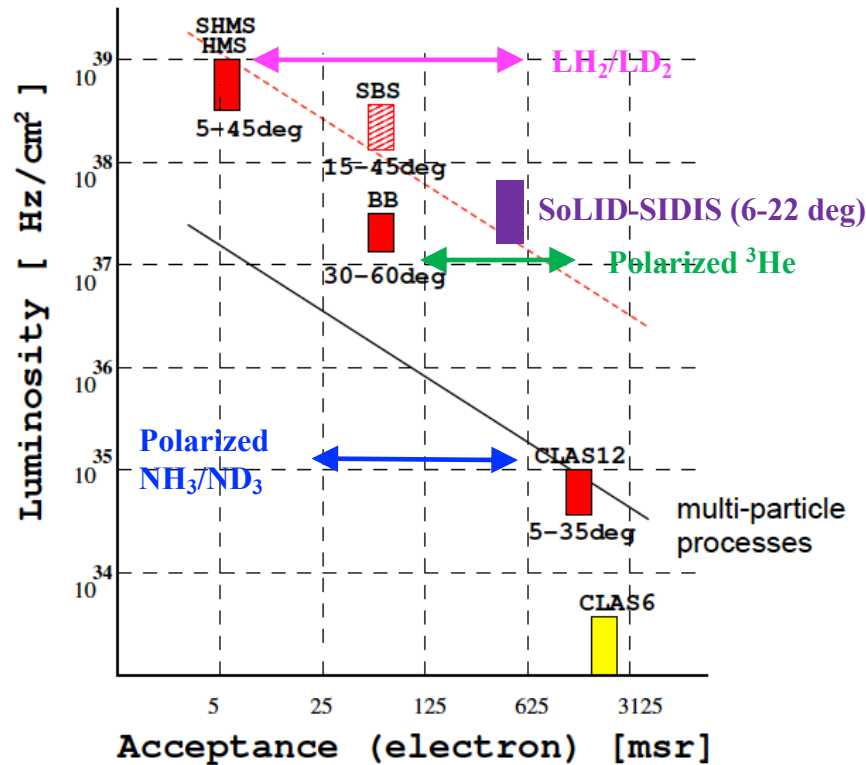
$$Q^2 = 2M\nu x_{Bj}$$

- Particles associated with the partonic (or other) degree of freedom that absorbed the virtual photon are found predominantly near the direction of the momentum transfer q
- *Partonic interpretation of electron scattering data is accessible at large $Q^2 \rightarrow$ particles of interest are located at forward angles and high momentum*



JLab detector landscape

Figure credit: B. Wojtsekhowski (JLab)



A range of 10^4 in luminosity.

A big range in solid angle:
from 5 msr (SHMS)
to about 1000 msr (CLAS12).

The SBS is in the middle:
for solid angle (up to 70 msr)
and high luminosity capability.

In several A-rated experiments
SBS was found to be the best
match to the physics.

GEM allows a spectrometer
with open geometry (->large
acceptance) at high L.

11/16/15

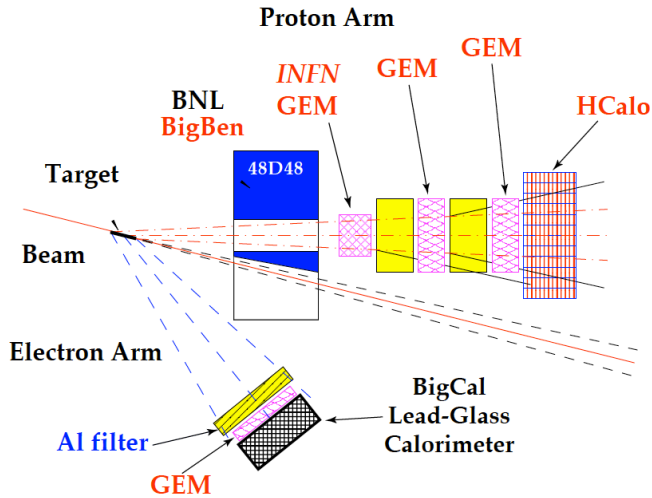
Super Bigbite Spectrometer Review

slide 9

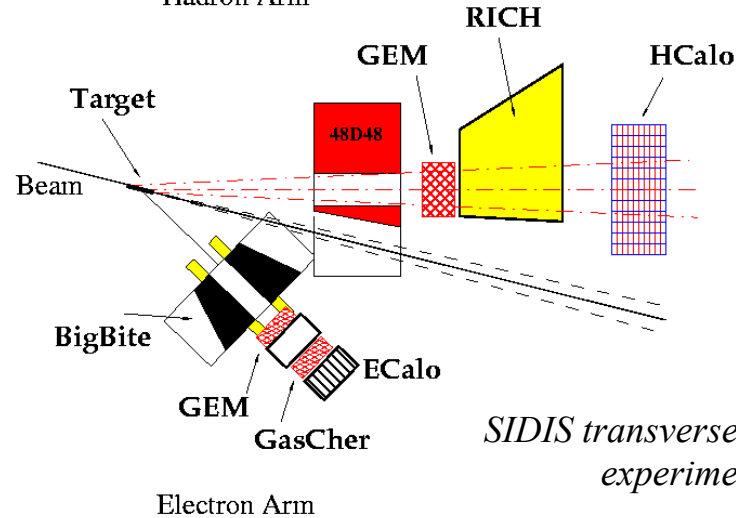
- Complementary equipment/capabilities of Halls A, B, C allow optimal matching of (Luminosity x Acceptance) of the detectors to the luminosity capabilities of the targets, including state-of-the-art polarized target technology.

The Super BigBite Spectrometer in Hall A

Proton form factors ratio, $G_E p(5)$ (E12-07-109)



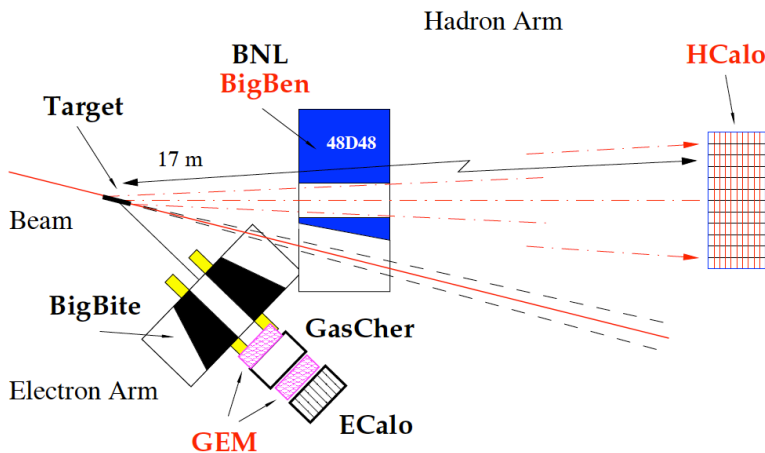
Hadron Arm



SIDIS transverse single-spin asymmetry experiment: E12-09-018

Electron Arm

Neutron form factors, E12-09-016 and E12-09-019



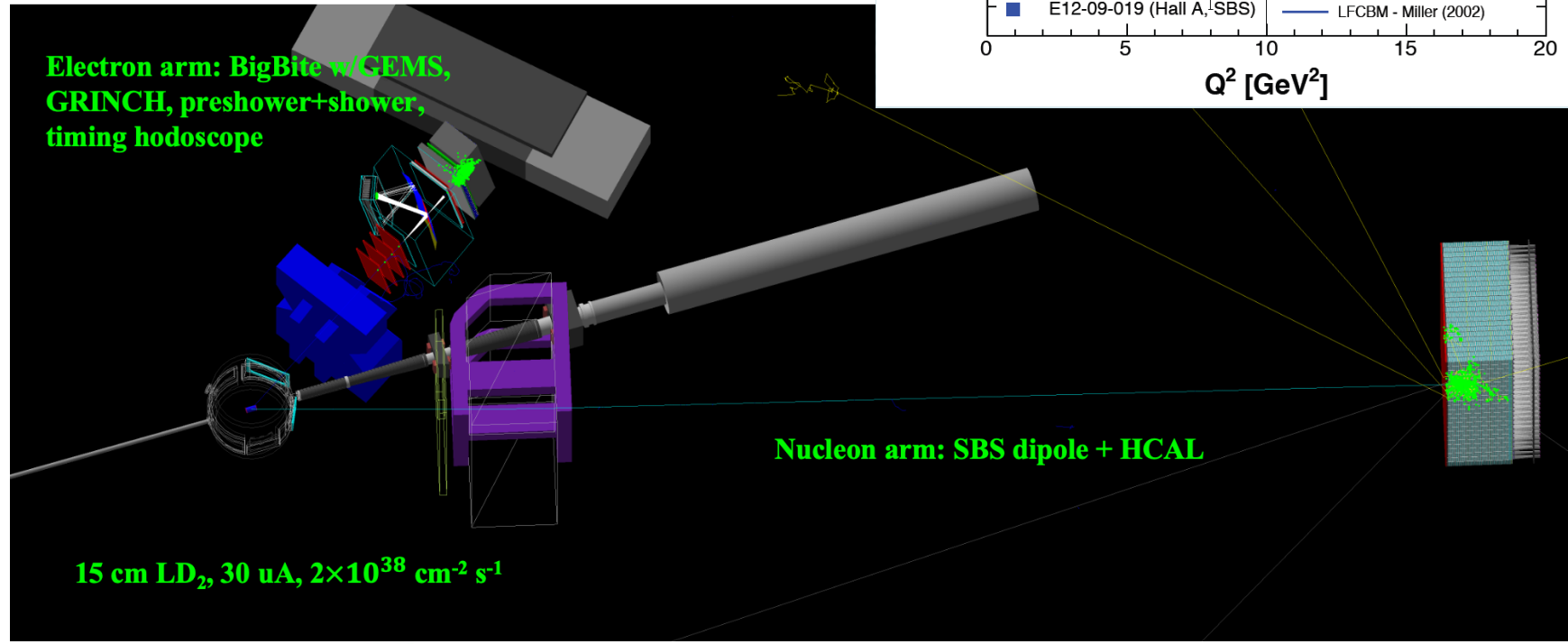
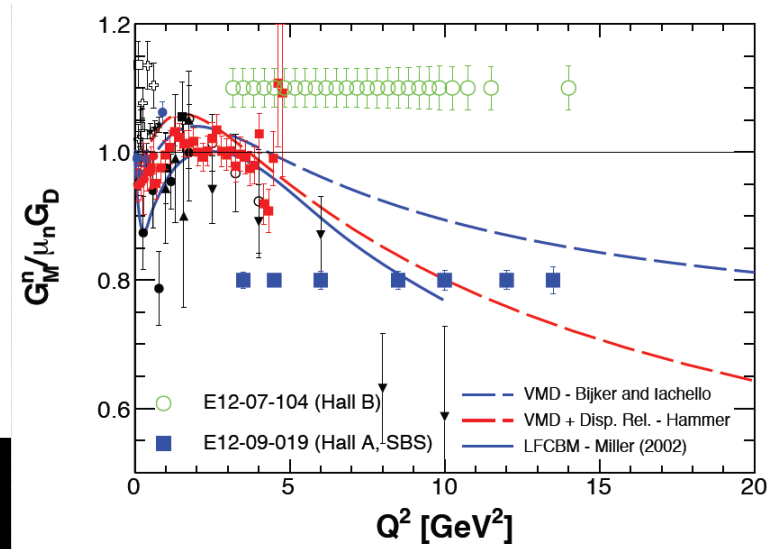
- What is SBS? → A 2.5 T*m dipole magnet with vertical bend, a cut in the yoke for passage of the beam pipe to reach forward scattering angles, and a flexible/modular configuration of detectors.
- Designed to operate at luminosities up to $10^{39} \text{ cm}^{-2} \text{ s}^{-1}$ with large momentum bite, moderate solid angle
- Time-tested “Detectors behind a dipole magnet”, two-arm coincidence approach—historically most productive in fixed-target expts.
- ***Large solid-angle + high luminosity @ forward angles = most interesting physics!***

Experiment E12-09-019 (GMN): First SBS experiment!

- Use ratio method on deuterium:

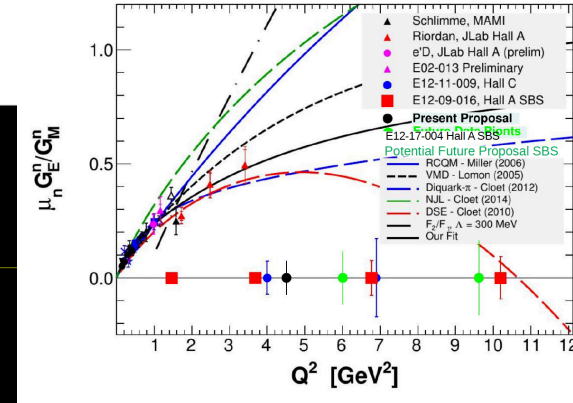
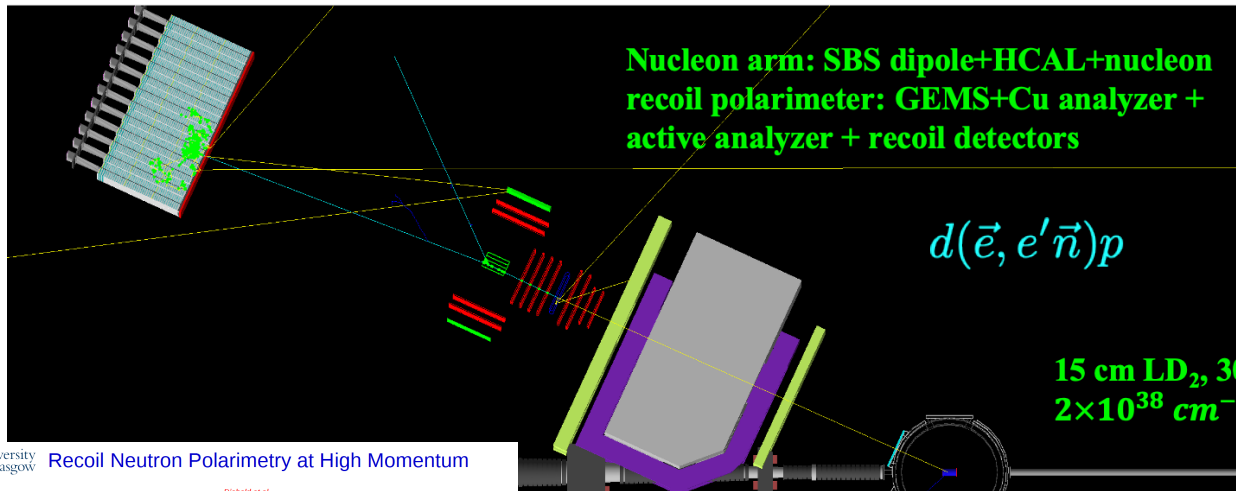
$$\frac{\sigma(d(e, e'n)p)}{\sigma(d(e, e'p)n)} \times \sigma(ep \rightarrow ep) \approx \sigma(en \rightarrow en)$$

- Small systematic uncertainties due to high proton and neutron efficiencies, good charge ID
- See Brian Quinn's talk for GMN status: Installation 2020!**



E12-17-004: GEN-RP

- World-leading measurement of $\frac{G_E^n}{G_M^n}$ at 4.5 GeV² and proof-of-concept for charge-exchange recoil polarimetry!
- See Will Tireman's talk and also recent [Dubna results on A_Y](#)



15 cm LD₂, 30 uA,
2 × 10³⁸ cm⁻²s⁻¹

University of Glasgow Recoil Neutron Polarimetry at High Momentum

- Until recently no data on n+C → n+p+X at several GeV/c (nor any nucleus)
- A_Y for np → np falling rapidly with increasing neutron momentum
- A_Y for charge-exchange np → pn large at sufficiently large t (θ_n ~ few deg.)
- σ_{np→np} factor ~10 higher than σ_{np→pn}

Elastic n-p Polarisation

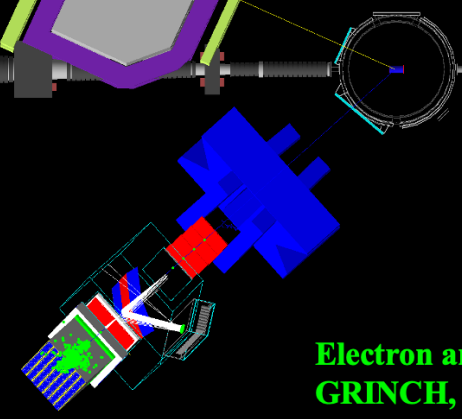
Forward Neutron np → np

Forward Proton np → pn

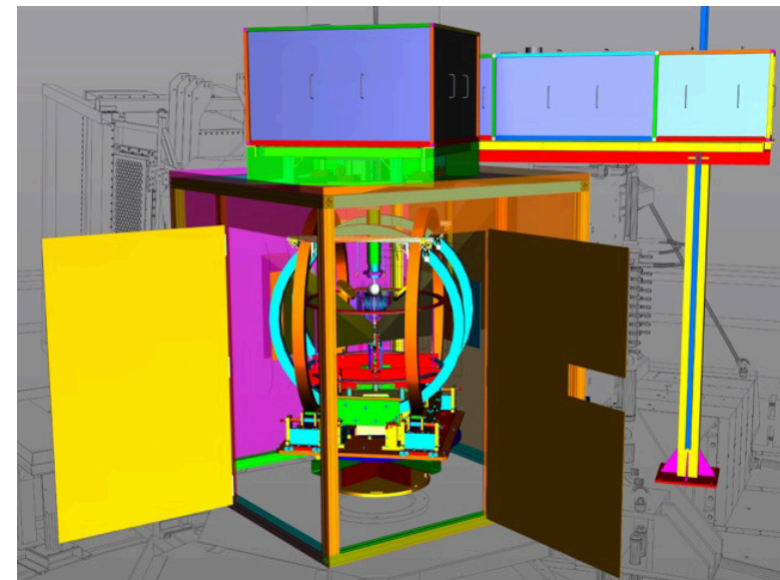
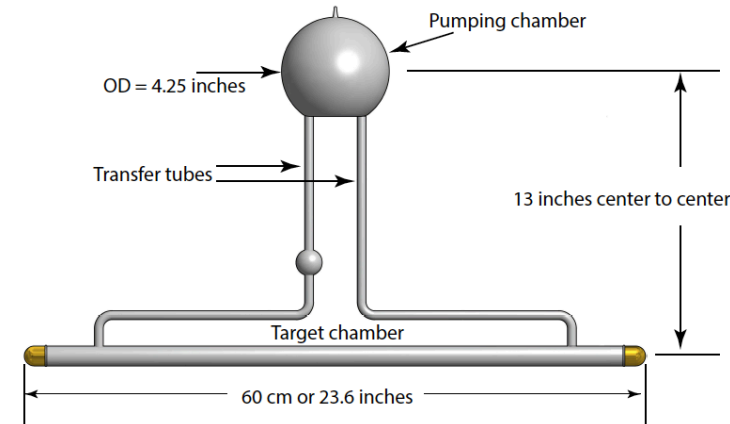
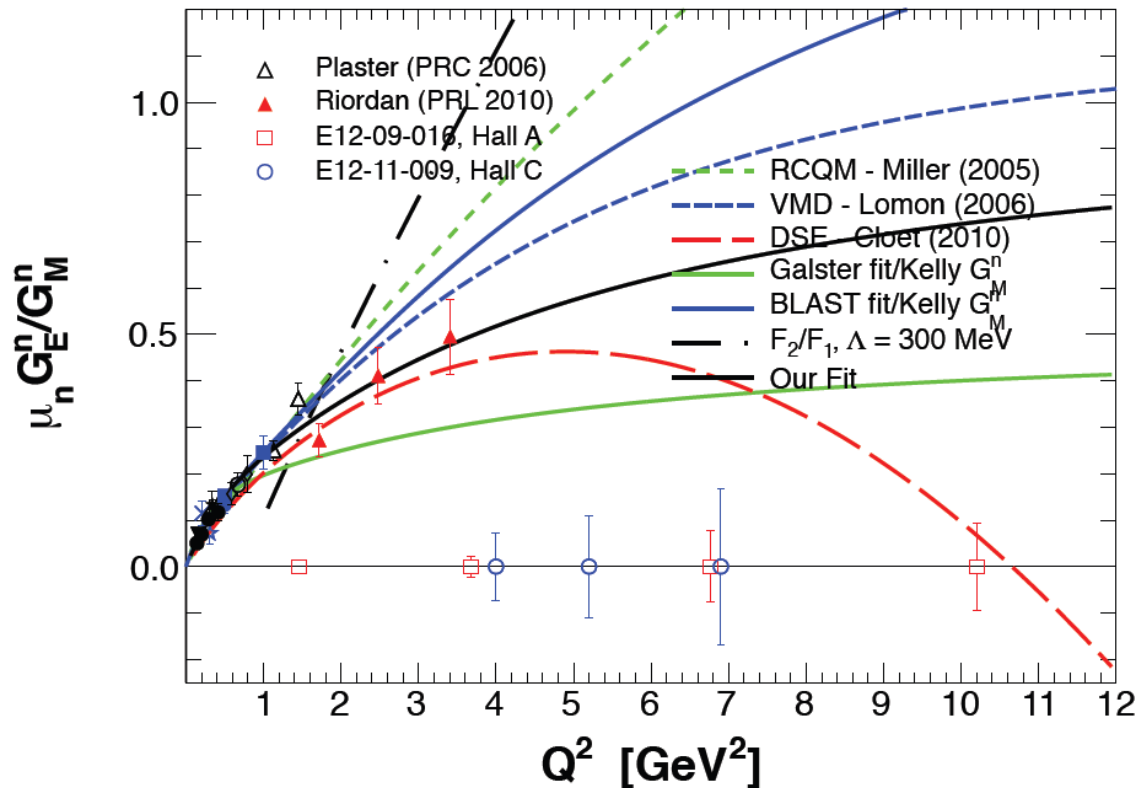
Abolins et al., PRL 30, 1973, 1183
Roberts et al., PLS31 (1970), 617

Diebold et al., PRD 25 (1970), 632
Fitz: Ludwig, JINR E13-96-123 (1999)

31st Jan 2019 GMn & GEN-Recoil Status Update 12



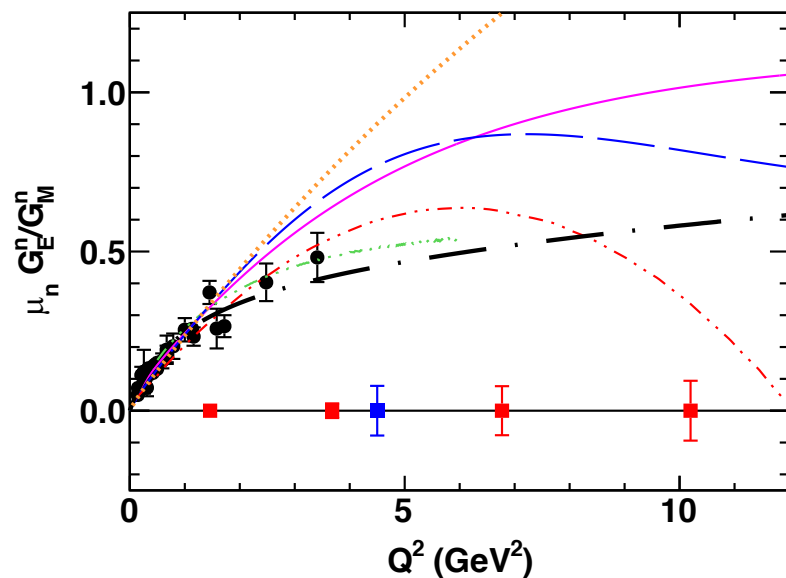
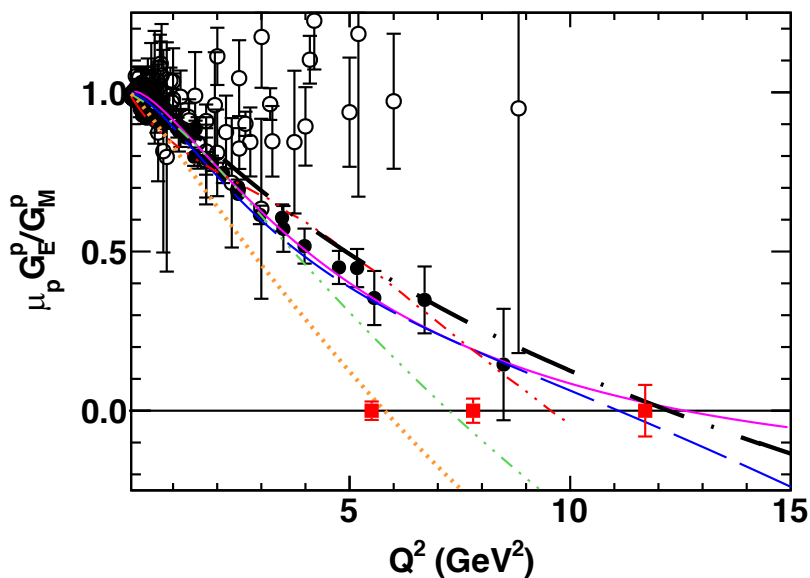
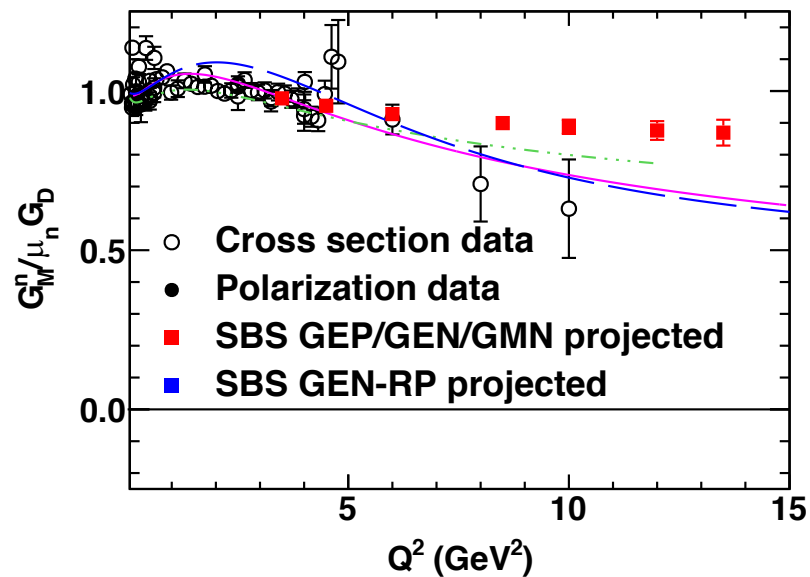
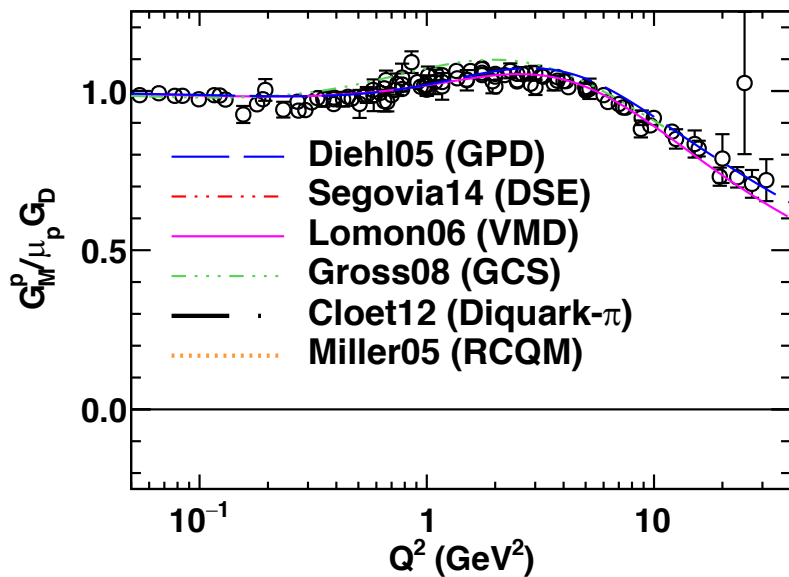
Experiment E12-09-016 (GEN)



Conceptual and Engineering Designs of Polarized ^3He target

- Upgraded, high-luminosity polarized ^3He target based on spin-exchange optical pumping and convection-driven circulation of polarized gas between optical pumping chamber and target chamber.
- **See Gordon Cates' talk!**

SBS Form Factor Program—Summary

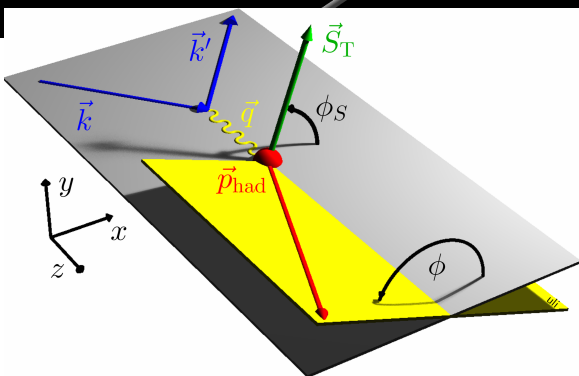
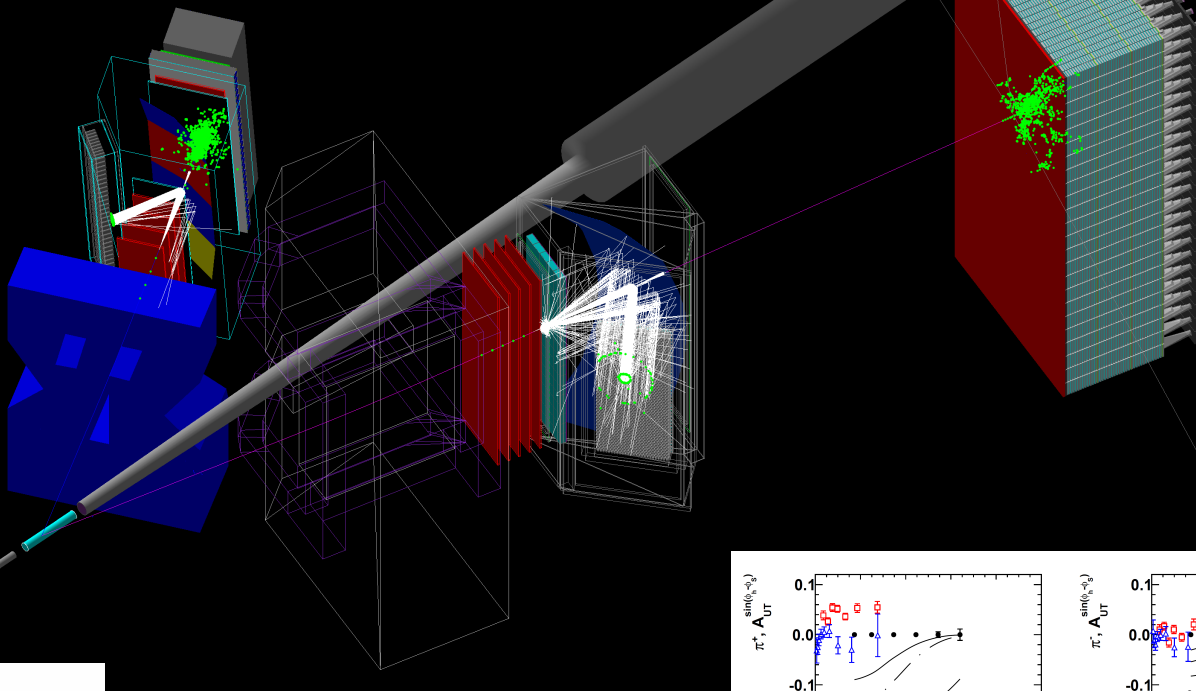


E12-09-018 (SIDIS/transversity)

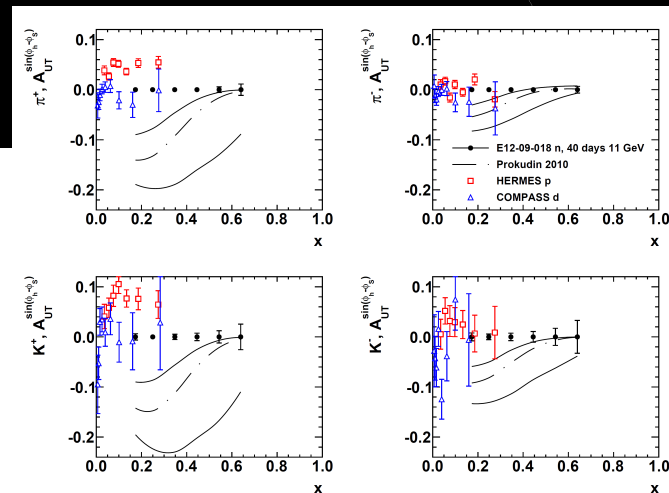
Electron arm: BigBite
@30 deg.

Hadron arm: SBS
@14 deg.

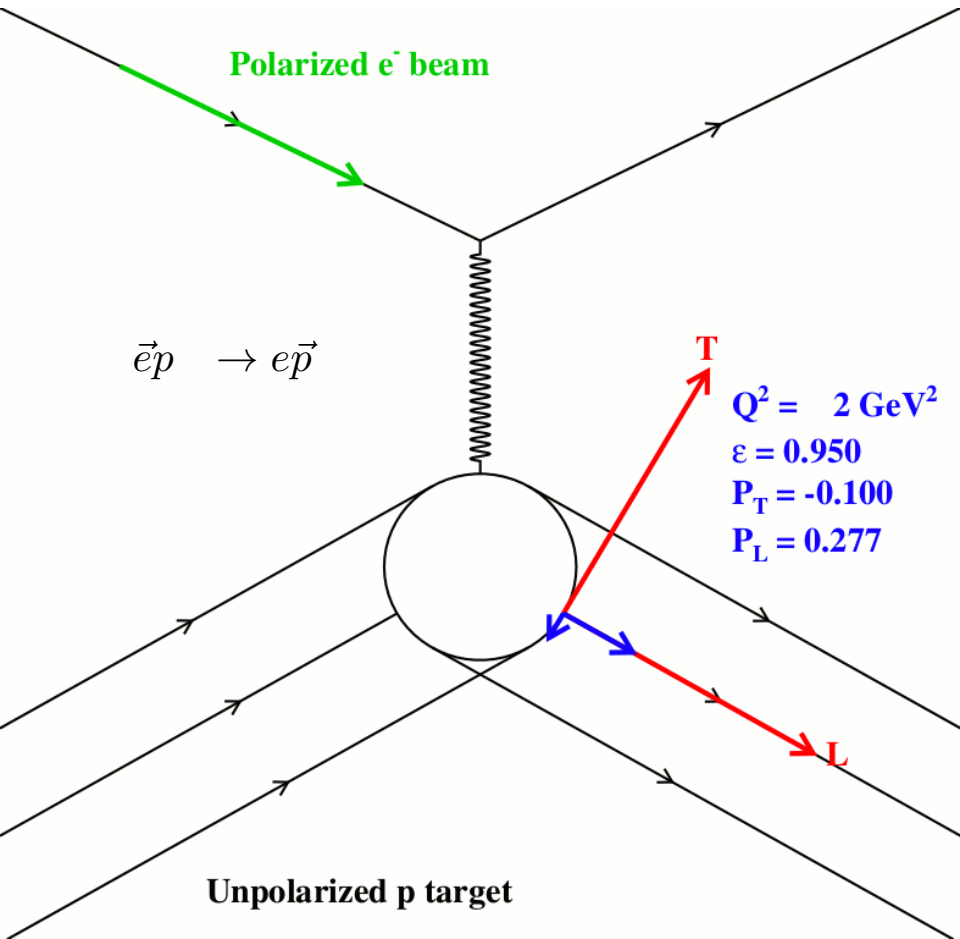
High-luminosity,
transversely polarized ^3He :
 $1.2 \times 10^{37} \text{ cm}^{-2} \text{ s}^{-1}$



- Approved 64 days, A- by PAC38.
- SIDIS transverse SSA (Collins, Sivers, etc.)
- **See Eric Fuchey talk!**



Polarization Transfer in Elastic eN scattering



$$P_t = -P_{beam} \sqrt{\frac{2\epsilon(1-\epsilon)}{\tau}} \frac{r}{1 + \frac{\epsilon}{\tau} r^2}$$

$$P_\ell = P_{beam} \frac{\sqrt{1-\epsilon^2}}{1 + \frac{\epsilon}{\tau} r^2}$$

$$P_n = 0$$

$$r \equiv \frac{G_E}{G_M}$$

$$\Rightarrow R_p \equiv \mu_p \frac{G_E^p}{G_M^p} = -\mu_p \sqrt{\frac{\tau(1+\epsilon)}{2\epsilon}} \frac{P_t}{P_\ell}$$

- Akhiezer and Rekalov (1968):
 - Derived relations between transferred polarization components in elastic eN scattering and the ratio of electromagnetic FFs $R = \mu G_E/G_M$*
- Perdrisat + Punjabi, 1993 proposal to CEBAF PAC: A *simultaneous* measurement of the two recoil polarization components in a polarimeter determines the FF ratio while canceling many systematic uncertainties (beam polarization, analyzing power, FPP instrumental asymmetry)

The ratio of transferred polarization components is directly proportional to G_E/G_M , and therefore much more sensitive to G_E at large Q^2 than the cross section

Recoil Proton Polarimetry: General Principles

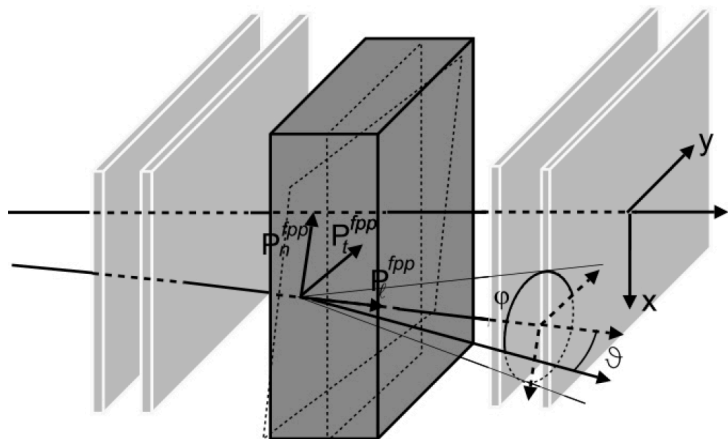


FIG. 9. Principle of the polarimeter, showing a noncentral trajectory through the front chambers, scattering in the analyzer, and a track through the back chambers; ϑ is the polar angle, and φ is the azimuthal angle from the y direction counterclockwise.

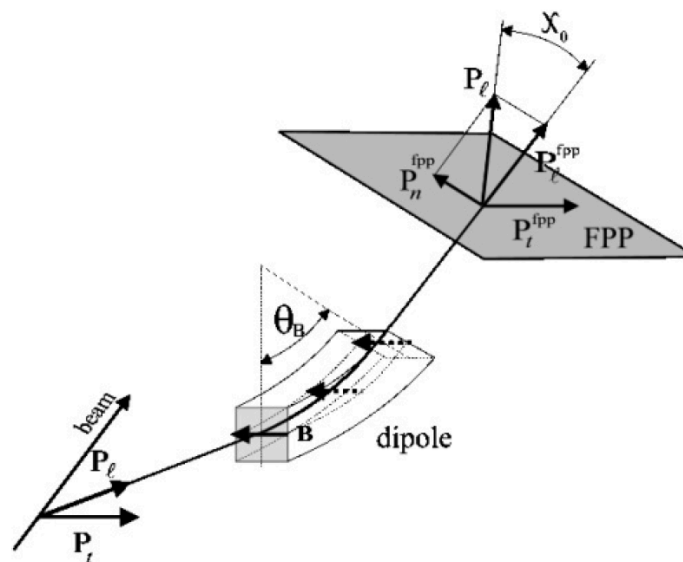
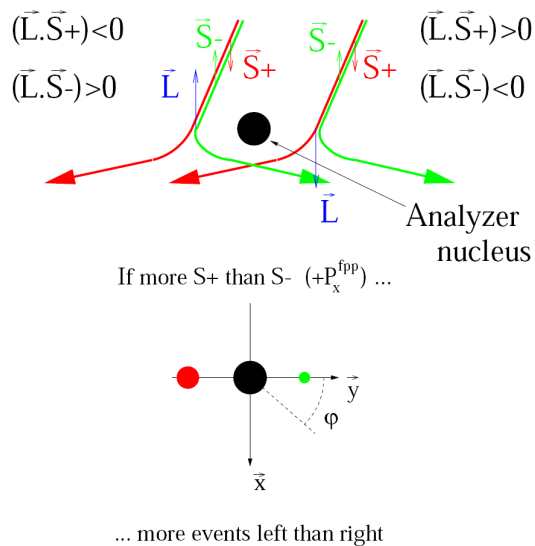


FIG. 15. Precession of the polarization component P_L in the dipole of the HRS by an angle χ_θ .

- Proton polarimetry via proton-nucleus scattering is based on the spin-orbit coupling in the nucleon-nucleon force.
- A spin-1/2 particle, such as a proton, is preferentially deflected by a spin-orbit force along the direction of $\vec{p} \times \vec{S}$, where \vec{p} is the incident proton momentum, and \vec{S} is the proton spin.
 - Note that a spin-orbit force is insensitive to longitudinal polarization!
 - Precession in spectrometer dipole field rotates P_L into a transverse component that can be measured
- By tracking the incident and scattered protons and measuring the azimuthal asymmetry in the angular distribution of secondary scatterings, the incident proton's (transverse) polarization is reconstructed

Statistical requirements: asymmetries vs. cross section measurements

Cross sections:

$$\sigma \propto N$$

$$\Rightarrow \frac{\Delta\sigma}{\sigma} = \frac{1}{\sqrt{N}}$$

To measure a cross section with a relative statistical precision of 1%, you need 10,000 events.

Asymmetries:

$$\Delta A = \sqrt{\frac{1 - A^2}{N}}$$

$$\frac{\Delta A}{A} = \sqrt{\frac{1 - A^2}{NA^2}}$$

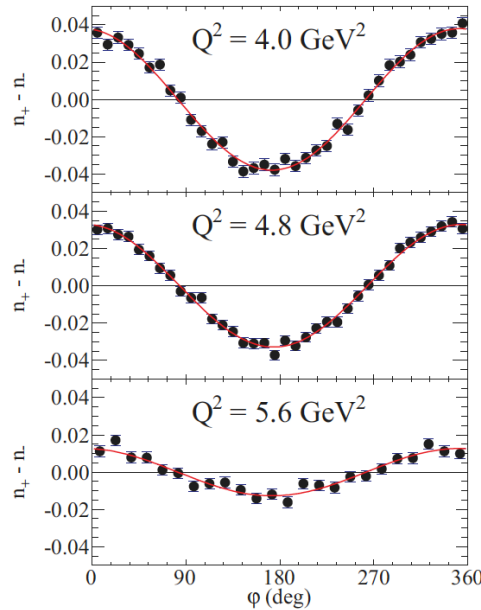


FIG. 6. (Color online) Focal-plane helicity-difference asymmetry $n_+ - n_- \equiv (N_{\text{bins}}/2)[N^+(\varphi)/N_0^+ - N^-(\varphi)/N_0^-]$, where N_{bins} is the number of φ bins and $N^\pm(\varphi)$, N_0^\pm are defined as in Eq. (4), for the three highest Q^2 points from GEp-II. Curves are fits to the data. See text for details.

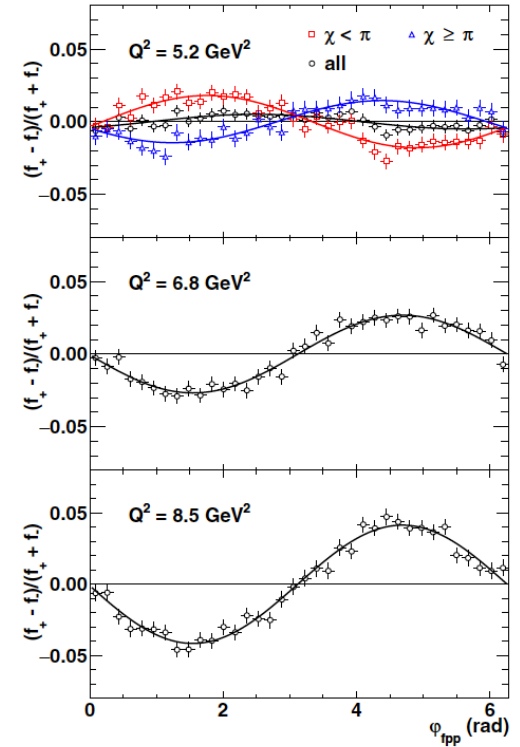
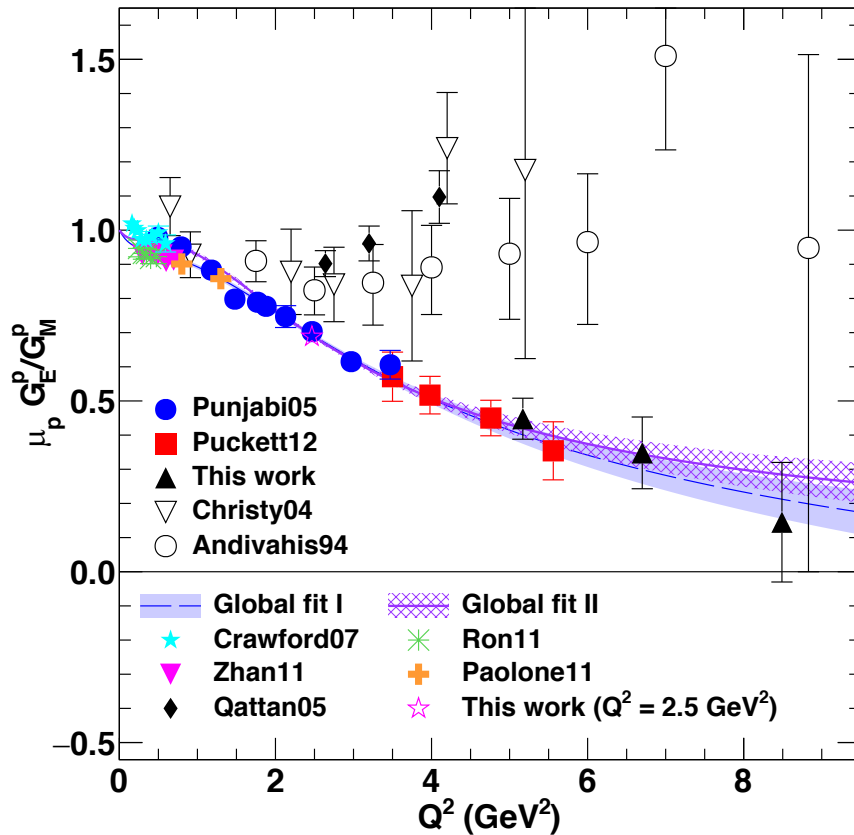


FIG. 10. Focal plane helicity difference/sum ratio asymmetry $(f_+ - f_-)/(f_+ + f_-)$, defined as in Eq. (20), for the GEp-III kinematics, for FPP1 and FPP2 data combined, for single-track events selected according to the criteria discussed in Sec. III B 2. Asymmetry fit results are shown in Table V. The asymmetry at $Q^2 = 5.2$ GeV² is also shown separately for events with precession angles $\chi < \pi$ and $\chi \geq \pi$, illustrating the expected sign change of the $\sin(\varphi)$ term.

- Typical asymmetry magnitude in a recoil proton polarimeter at "high" momentum is ~few percent.
- For example: to measure a 5% asymmetry with a relative precision of 1%, one needs $N = 10,000 \times \frac{1-A^2}{A^2} \approx 4 \times 10^6$ events!

→ Asymmetry measurement must maximize beam and/or target polarization, and luminosity × acceptance!

G_E^p/G_M^p polarization transfer data are among the most-cited JLab results



- **Gep-I:**
 - Jones *et al.*, *Phys. Rev. Lett.* **84** (2000) 1398-1402: **880 INSPIRE-HEP citations**
 - Punjabi *et al.*, *Phys.Rev.* **C71** (2005) 055202: **442 INSPIRE-HEP citations**
- **Gep-II:**
 - Gayou *et al.*, *Phys.Rev.Lett.* **88** (2002) 092301: **809 INSPIRE-HEP citations**
 - Puckett *et al.*, *Phys.Rev.* **C85** (2012) 045203: **145 INSPIRE-HEP citations**
- **Gep-III/Gep-2γ:**
 - Puckett *et al.*, *Phys.Rev.Lett.* **104** (2010) 242301, **262 INSPIRE-HEP citations**
 - Meziane *et al.*, *Phys.Rev.Lett.* **106** (2011) 132501, **82 INSPIRE-HEP citations**
 - Puckett *et al.*, *Phys.Rev.* **C96** (2017) no.5, 055203, **31 INSPIRE-HEP citations**
- **Low- Q^2 data from JLab:**
 - Ron *et al.*, *Phys.Rev.Lett.* **99** (2007) 202002, **70 INSPIRE-HEP citations**
 - Ron *et al.*, *Phys.Rev.* **C84** (2011) 055204, **98 INSPIRE-HEP citations**
 - Zhan *et al.*, *Phys.Lett.* **B705** (2011) 59-64, **181 INSPIRE-HEP citations**
 - Paolone *et al.*, *Phys.Rev.Lett.* **105** (2010) 072001, **91 INSPIRE-HEP citations**

• *Extraction of the same physical property of the proton from different experimental observables yields different results!*

• Guichon and Vanderhaeghen, *PRL* 91, 142303 (2003): “*This discrepancy is a serious problem as it generates confusion and doubt about the whole methodology of lepton scattering experiments.*”

• Discrepancy still not yet fully understood

• Unexpected results of GEP experiments have changed our basic notions about proton structure!

2017 Tom W. Bonner Prize in Nuclear Physics Recipient

Charles F. Perdrisat
College of William and Mary

Citation:

"For groundbreaking measurements of nucleon structure, and discovering the unexpected behavior of the magnetic and electric nucleon form factors with changing momentum transfer."



Background:

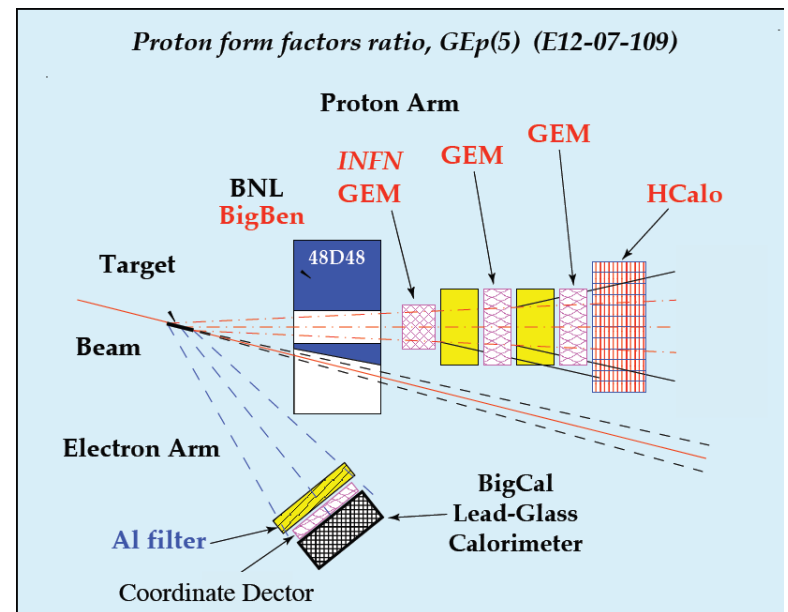
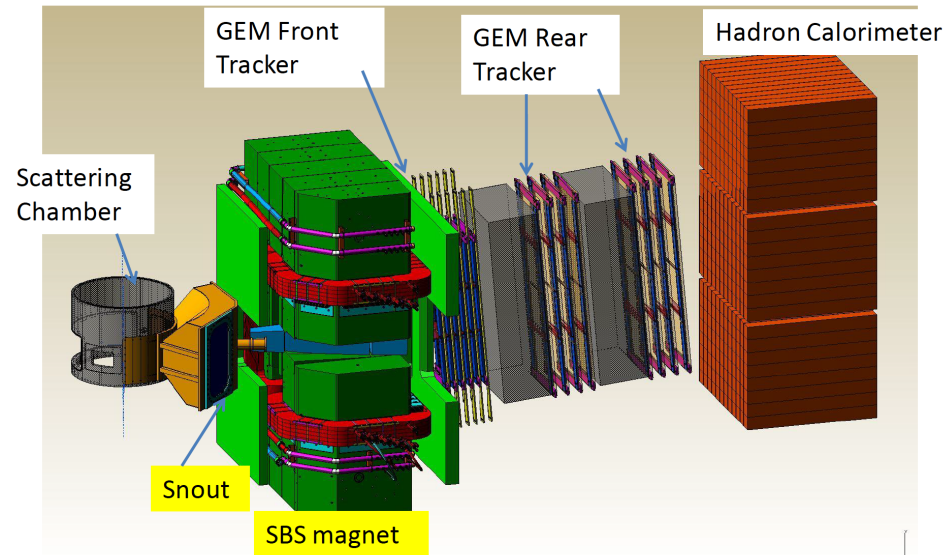
Charles F. Perdrisat, Ph.D., was a professor at the College of William and Mary (Williamsburg, Va.) for the last 50 years having retired earlier this year. Throughout his career, Dr. Perdrisat's research focus included nuclear reactions with proton and deuteron beams, both polarized and unpolarized. He conducted research at SATURNE in Saclay, France, TRIUMF in Vancouver, B.C., LAMPF in Los Alamos, New Mexico, Brookhaven National Laboratory in Upton, N.Y., and JINR in Dubna, Russia. During the last half of his career, he was committed to the investigation of the structure of the proton at Jefferson Laboratory, concentrating in obtaining polarization transfer data in the scattering of polarized electrons on unpolarized protons. These data, from 3 distinct experiments organized in close collaboration with Vina Punjabi, Ph.D., Mark K. Jones, Ph.D., Edward J. Brash, Ph.D., and Lubomir Pentchev, Ph.D., have resulted in a significant change of paradigm in the understanding of the structure of the nucleon. After completing his undergraduate training in physics and mathematics at the University of Geneva in 1956, Dr. Perdrisat became an assistant in the physics department at the Swiss Federal Institute of Technology in Zurich) in Switzerland, under Prof. Paul Scherrer; he received his Ph.D. in 1962. He completed a three-year postdoctoral fellowship at the University of Illinois Urbana-Champaign, before heading to William and Mary in 1966.

Selection Committee:

2017 Selection Committee Members: Rocco Schiavilla (Chair), D. Hertzog, P. Jacobs, Kate Jones, I-Y. Lee

How to reach higher Q^2 ?

- Increase beam energy \rightarrow Increase kinematically accessible Q^2 range; increase cross section for constant Q^2
- Elastic ep cross section scales as $\sigma \approx E^2/Q^{12}$
- FPP efficiency is roughly Q^2 -independent
- FPP analyzing power scales roughly as $\frac{1}{p_p} \approx M/Q^2$
- Statistical FOM scales as $NA_y^2 \approx E^2/Q^{16}$
- Increase beam polarization? 80% \rightarrow 100% would only increase FOM by 1.6
- Increase luminosity? Best possible at JLab 12 GeV $\sim 10^{39} \text{ cm}^{-2} \text{ s}^{-1}$; (factor of 2 above 6 GeV expt's).
- Most room for growth? \rightarrow **Increase solid angle/ Q^2 acceptance!**
 - **2X increase in target thickness and solid angle from 6 \rightarrow 35 msr leads to \sim 30X gain in figure-of-merit**
- JLab PAC-approved G_E^p experiment: E12-07-109; 45 days in Hall A
 - $\Delta(\mu G_E/G_M) \sim 0.07 @ Q^2 = 12 \text{ GeV}^2$
 - “High impact experiment” designation from PAC41 in 2013



Experiment E12-07-109 (GEP)

Electron arm: High-temperature lead-glass EM calorimeter (ECAL) and scintillator based coordinate detector (CDET)

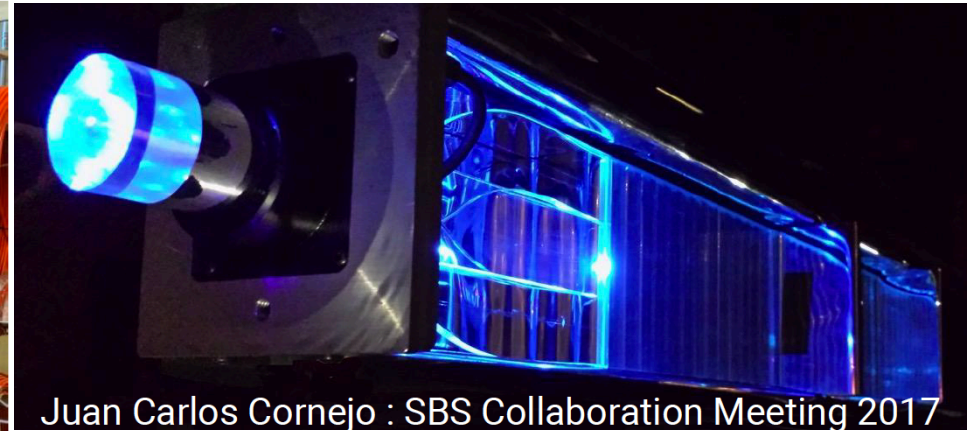
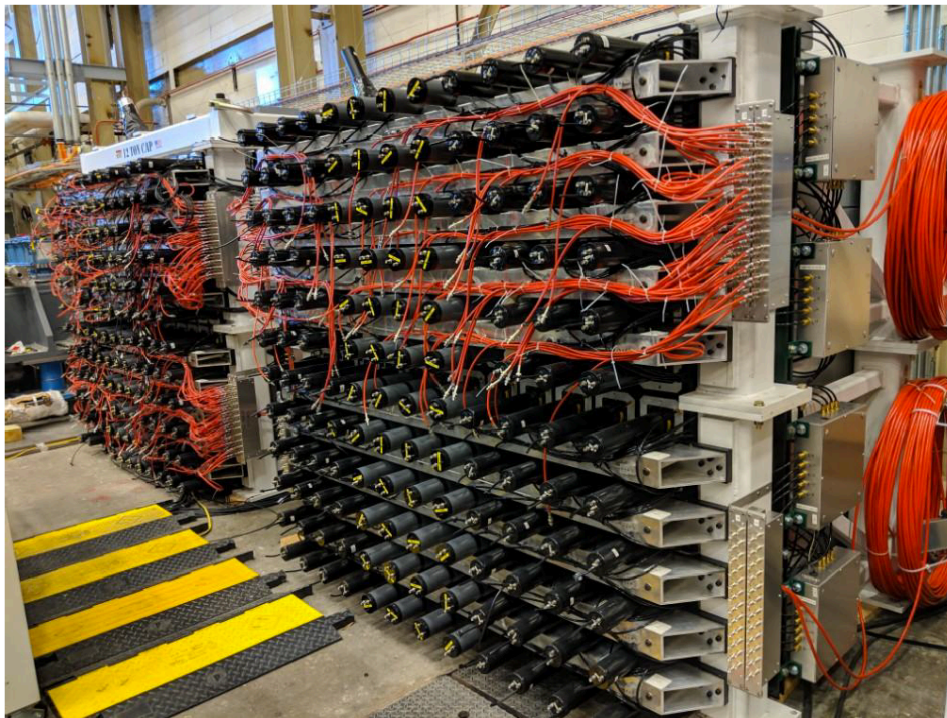
30-cm liquid hydrogen target, 75 μA beam current: Luminosity $6 \times 10^{38} \text{ cm}^{-2}\text{s}^{-1}$

Proton Arm: SBS dipole magnet, GEM trackers and CH_2 analyzers for proton polarimetry, iron-scintillator HCAL for trigger

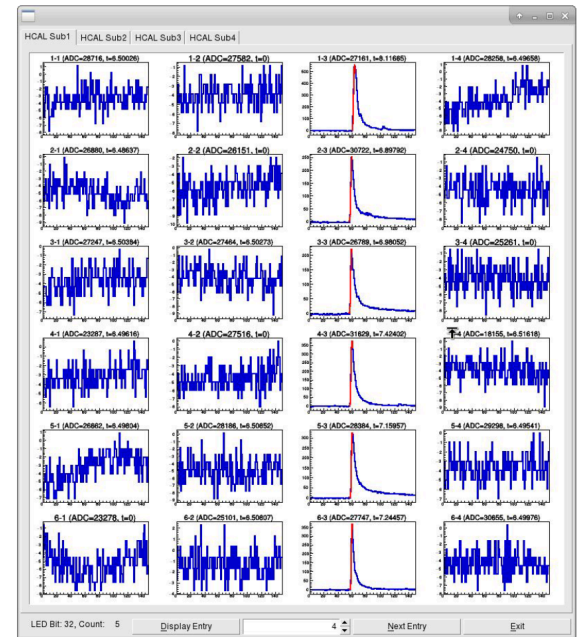
(Screenshots from SBS GEANT4 simulation)

- Original motivation for SBS concept. Approved PAC32 (2007), A-. PAC35 reduced max. Q^2 to 12 GeV^2 and beam time allocation to 45 days.
- **“High impact experiment” designation from PAC41**

The SBS Hadron Calorimeter



Juan Carlos Cornejo : SBS Collaboration Meeting 2017



1

- Iron-Scintillator sampling calorimeter with high (and similar) efficiency for protons and neutrons, and other high-energy hadrons
- Threshold $\sim 50\%$ of mean elastic proton signal
- Used in all SBS experiments
- Important for trigger and constraining high-rate tracking in GEP, SIDIS, and GEN-RP

Cosmic ray tracks through HCAL

The High-Temperature ECAL (Proof of Concept)

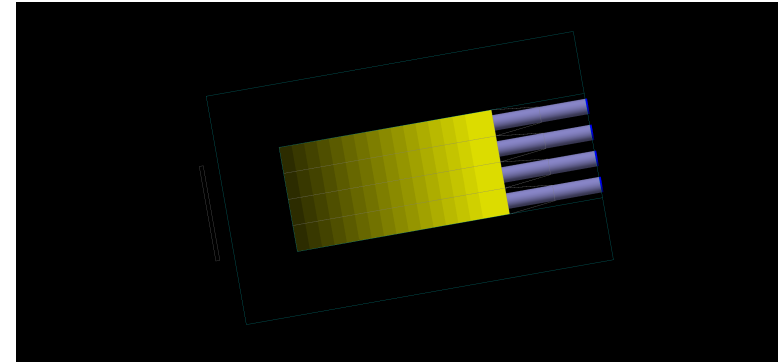
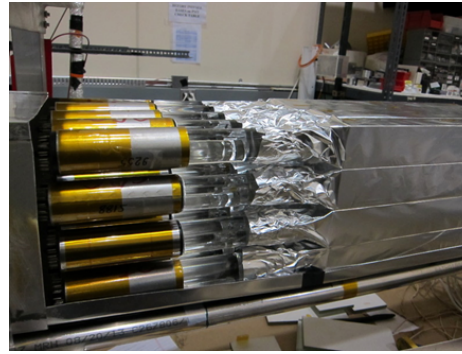
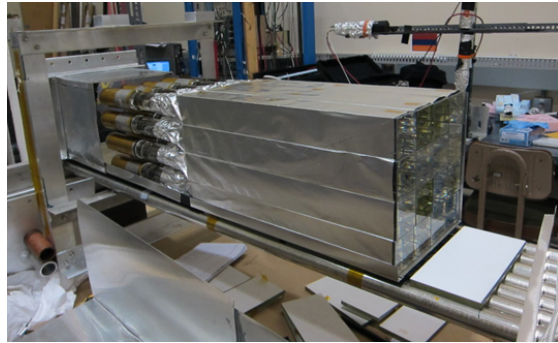


Figure 1 Photo of C16 lead glass blocks, light guide and PMTs.

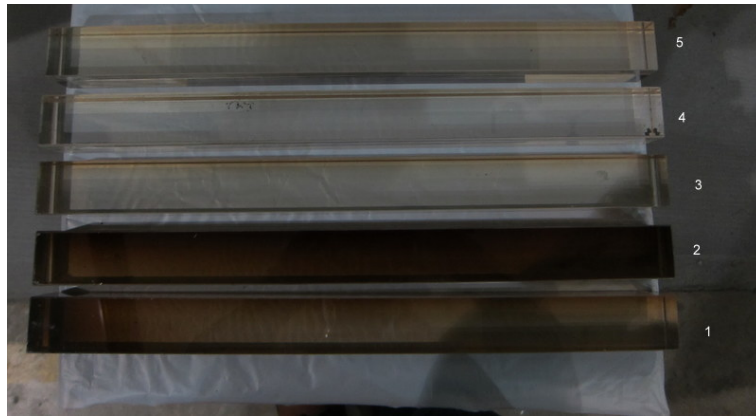
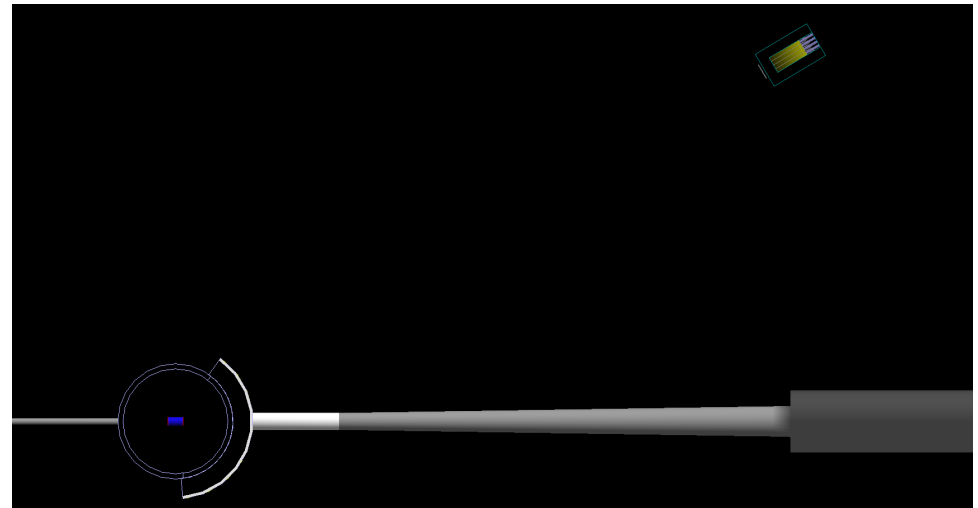
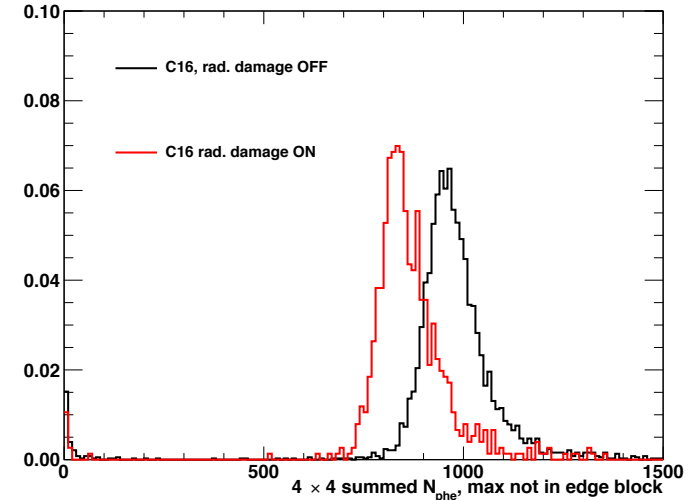
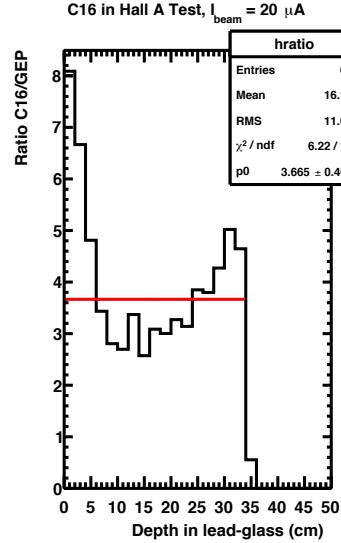
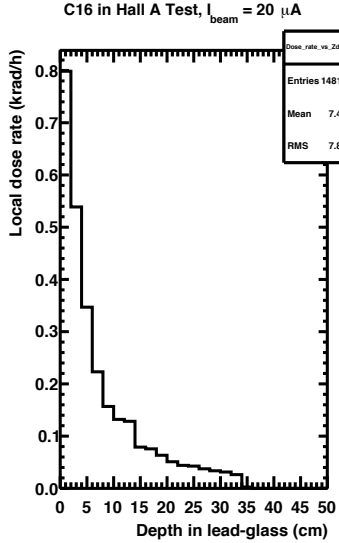
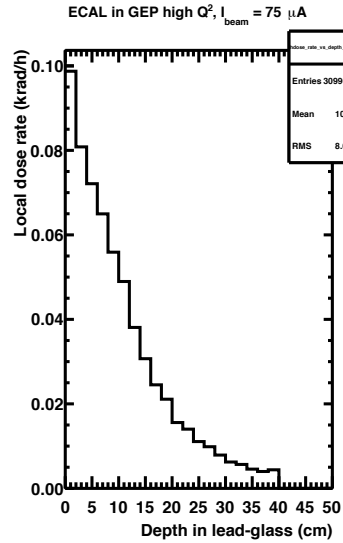


Figure 6 The lead glass blocks used to monitor the radiation dose after the C16 was placed at 10° and there was $20\mu\text{A}$ beam on the 15cm LH2 target. Block 1 was placed parallel to the C16 along the beamline side of the C16. Block 1 has damage at the front (left side of photo) and along the side. Block 2 was placed in front of the C16 and perpendicular to the front face. Blocks 3,4 and 5 were located at different locations on the spectrometer platform that was near 30° . These blocks show only moderate damage.

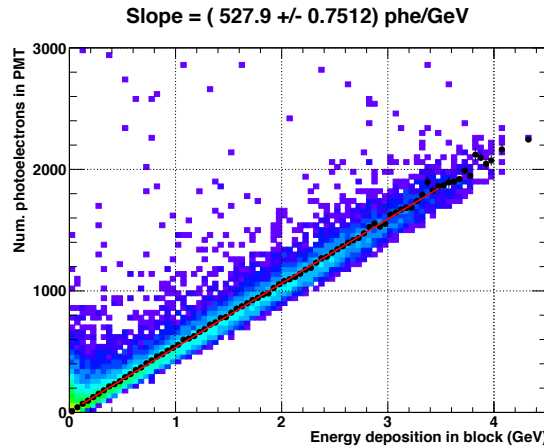
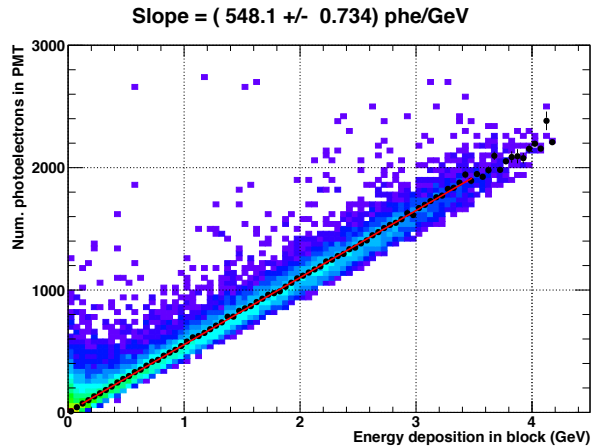


- 16-block thermal annealing prototype test in Hall A with 250°C oven, 2015
- GEANT4 simulation with model for radiation-induced transparency reduction

Benchmarking Thermal Annealing Model

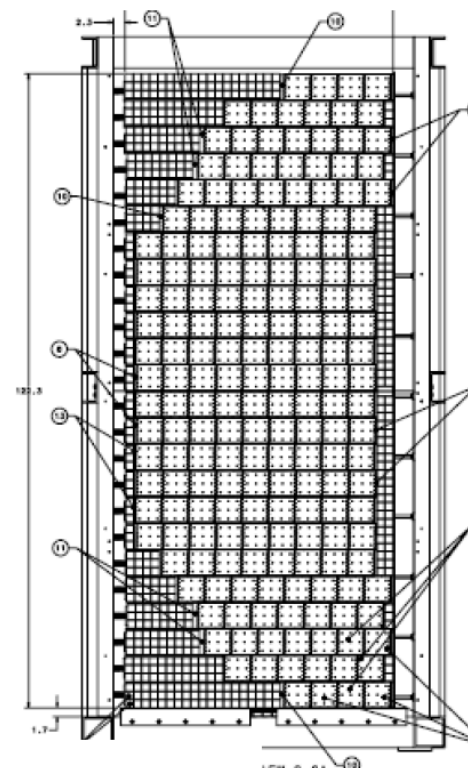
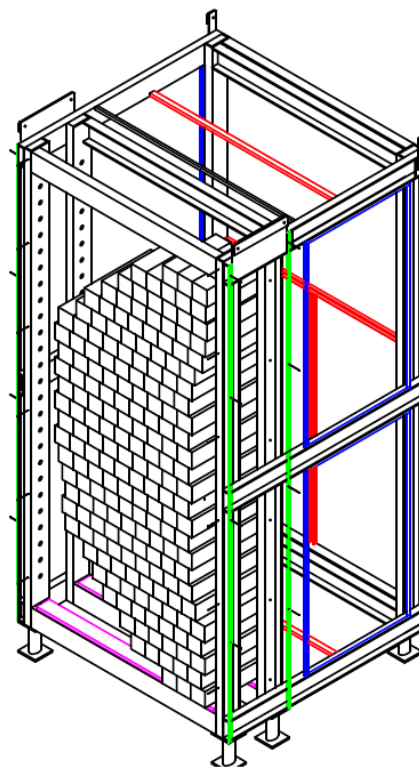
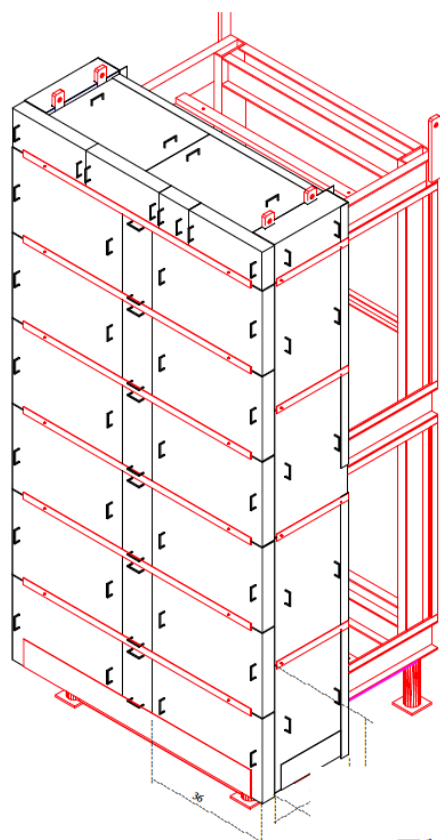


- Radiation dose rate during C16 test $\sim 8X$ higher (at front of glass) than expected in GEP ECAL
- Radiation damage model calibrated to reproduce C16 test data.
- **Predicts equilibrium state during GEP of $(96.3 \pm 0.2)\%$ of undamaged signal**



The High Temperature ECAL, I

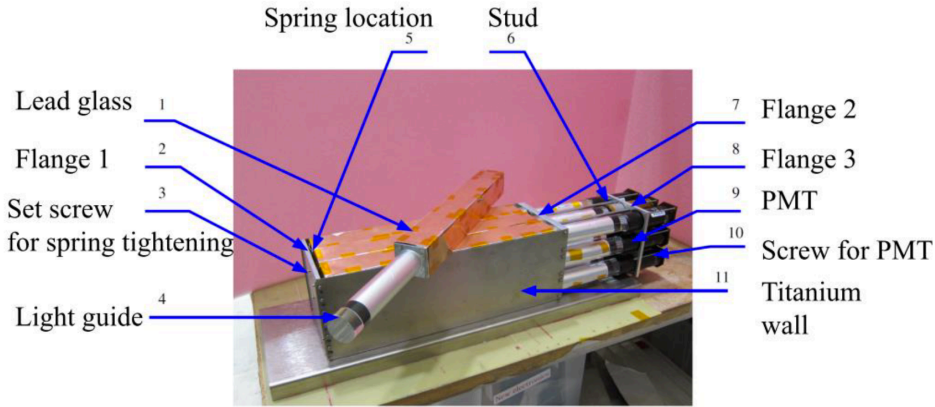
Electron arm calorimeter in the model



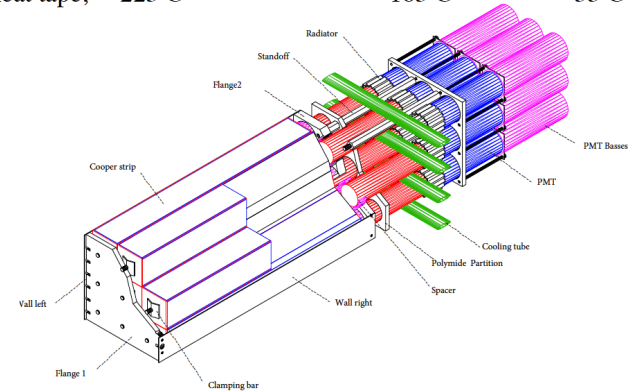
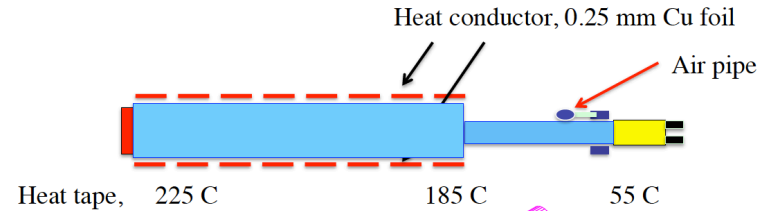
1737 lead-glass modules

Elevated temperature of the glass (225-185 C)
provides **continuous** annealing of radiation damage

The High Temperature ECAL, II



Electron arm: Calorimeter's temperature, 3x3 group



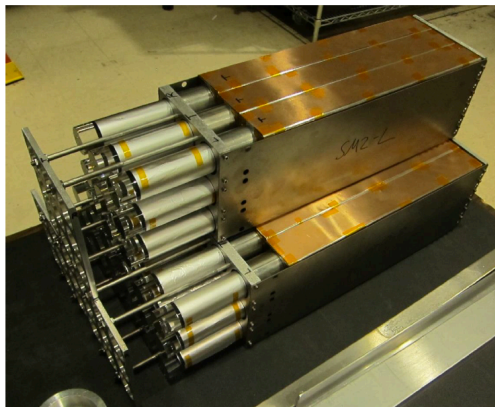
GEP/SBS B.Wojtsekhowski

PAC47 July 30, 2019

23

Work since Feb SBS meeting

- 126 of out 191 supermodules have been assembled
- JLab Detector Support Group is contributing manpower to assembling supermodules.

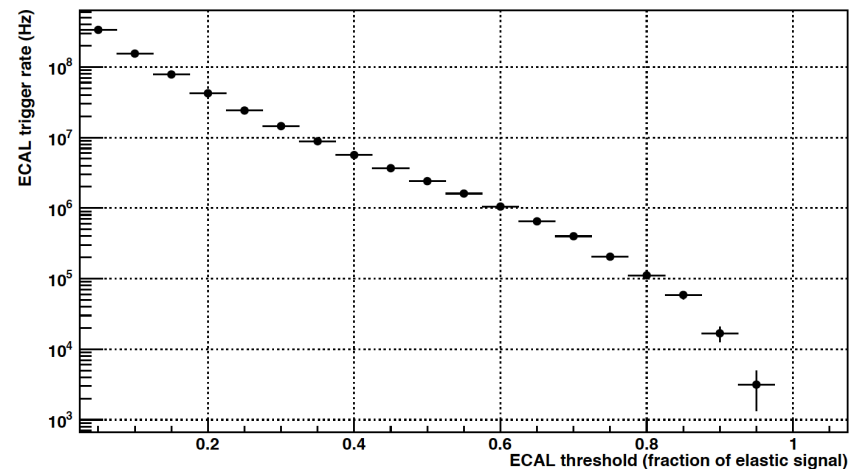
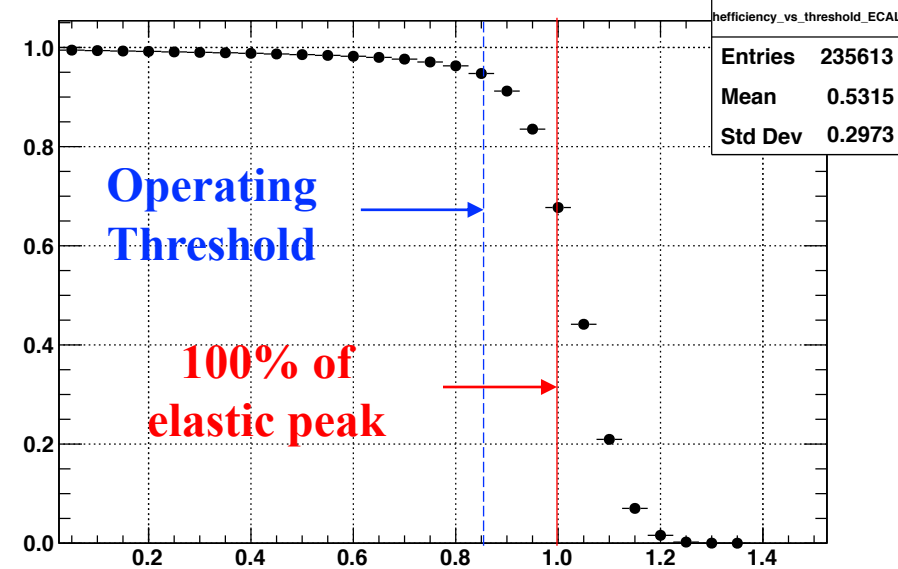


7

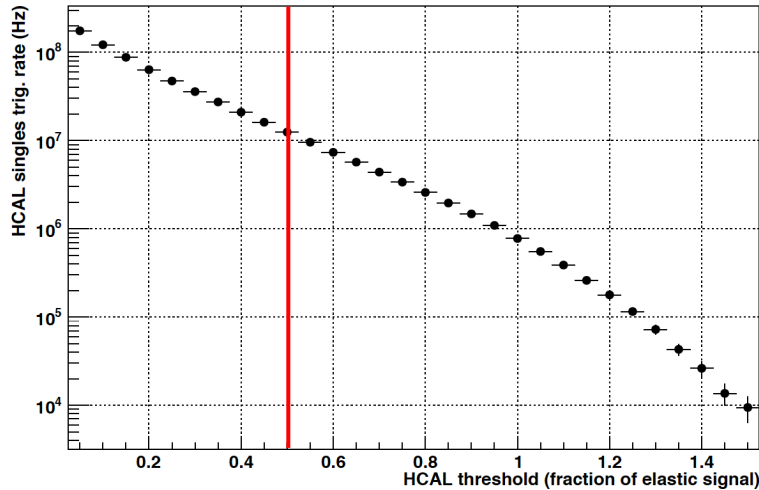
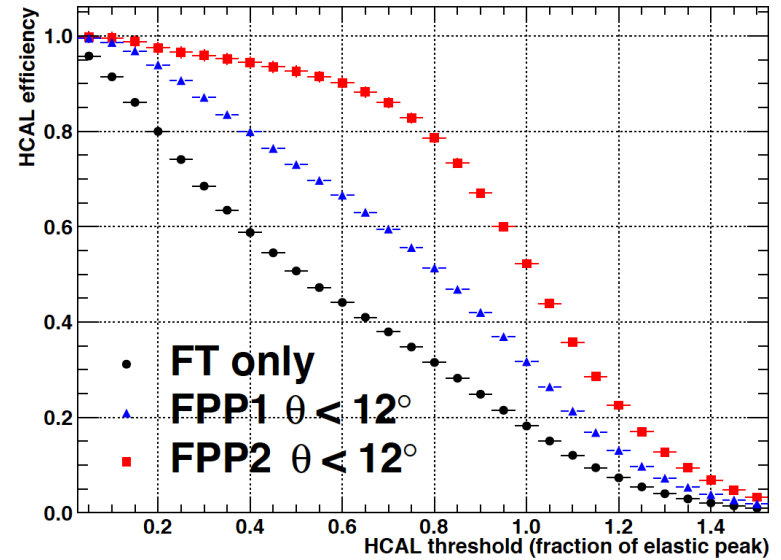
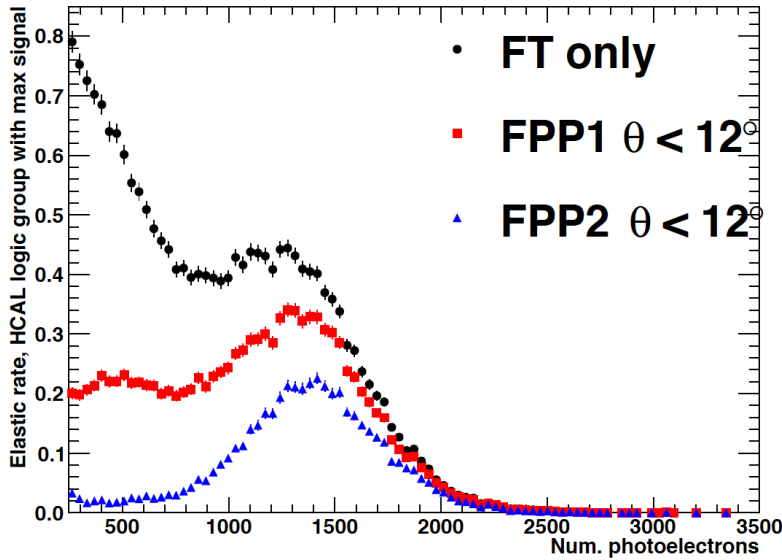
- Contributions from: NCCU, JLab, YerPhi, SBU, UVA, JMU, UConn, Glasgow, INFN, CMU, NCAT
- NCCU received large NSF grant to design and construct ECAL oven

Logic of the GEP Trigger/DAQ, I: ECAL

- Trigger for GEP is based on exclusive two-body final state and total absorption calorimeters for both final-state particles, with high threshold
- Raw data rate dominated by $\sim 150,000$ individual GEM readout strips, each firing at high rate ("online" occupancy approaching 100%)
- Need as-selective-as-possible trigger, for inelastic background suppression but especially for data rate management.
- ECAL trigger is based on overlapping sums of 32 (4 horizontal x 8 vertical)
- High-temperature ECAL maintains stable energy resolution of lead-glass at $\frac{\sigma_E}{E} \approx 6\%$
 - \rightarrow Trigger threshold as high as 80-85% of elastic electron energy (equivalent) at efficiency $\geq 95\%$
- Singles rate ~ 100 kHz

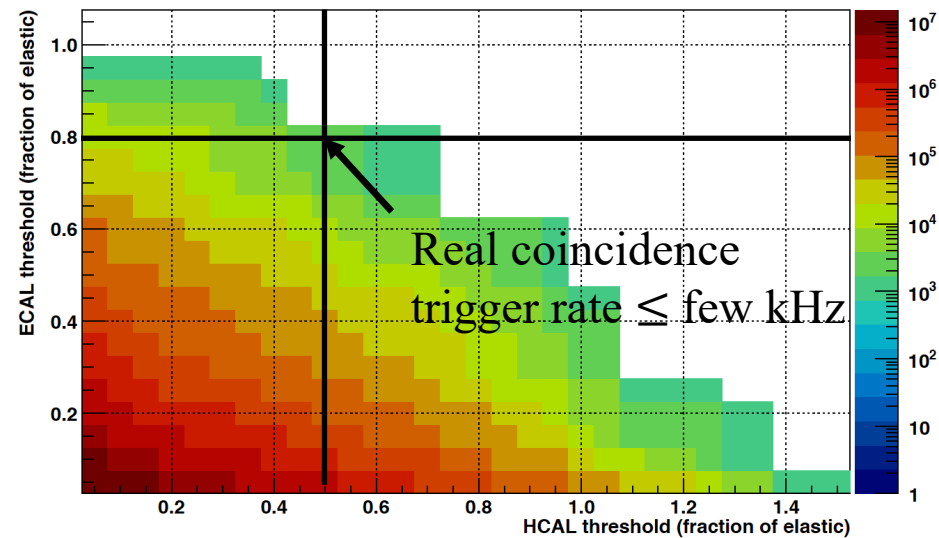
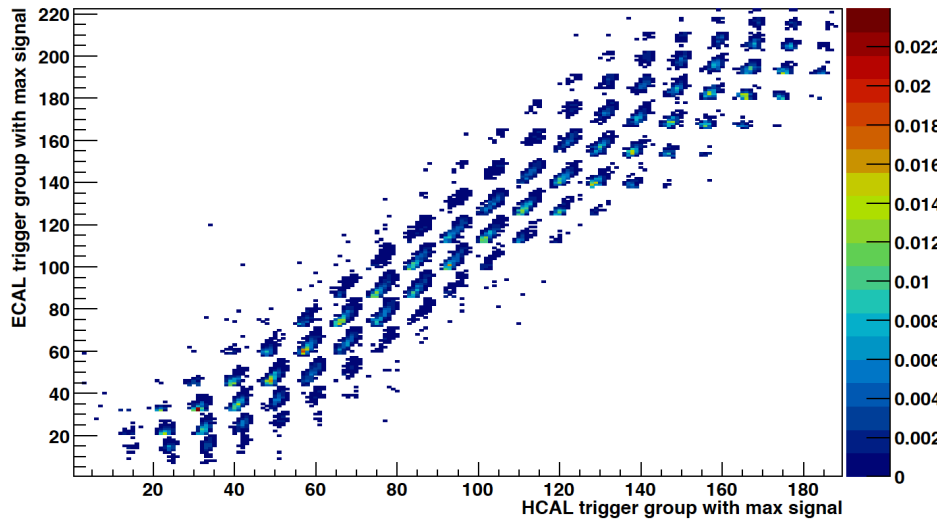


Logic of the GEP Trigger/DAQ, II: HCAL



- HCAL single-arm trigger is formed from an “OR” of all possible (overlapping) sums of 4×4 modules (rate vs threshold below, left), ~ 10 MHz at threshold approximately 50% of average elastic proton signal (above, left)
- “Efficiency” for HCAL trigger (above, right) is complicated because it is located *behind* the proton polarimeter (GEM chambers plus CH_2 analyzers)
- Efficiency of HCAL trigger for events of interest for polarimetry is high ($\geq 90\%$)
- HCAL trigger *may* actually *increase* polarimeter FOM by preferentially selecting events with high analyzing power:
 - See <https://arxiv.org/abs/1908.06159>

Logic of the GEP Trigger/DAQ, III: "Level 2" coincidence



- To get from ~ 100 kHz ECAL single-arm trigger rate to < 5 kHz event rate to disk/tape, we implement ep angular correlation in the coincidence trigger.
- To define the coincidence trigger logic, we simulate the single-arm trigger logic with elastic ep scattering events, and plot the correlation between the respective HCAL and ECAL sums with largest signals.
- We then create a look up table consisting of a list for each HCAL sum of all ECAL sums containing at least 0.1% of the total elastic yield (for that HCAL sum).
- The "level 2" coincidence trigger then requires at least one ECAL-HCAL "match" above threshold within this lookup table.
- The "real" coincidence rate due to inelastic events with this logic is ~ 3 kHz at the nominal thresholds, with another 1-2 kHz of accidental coincidences for a 30-ns coincidence timing window

Gas Electron Multipliers (GEMs): High-Rate, High Resolution Charged-Particle Tracking

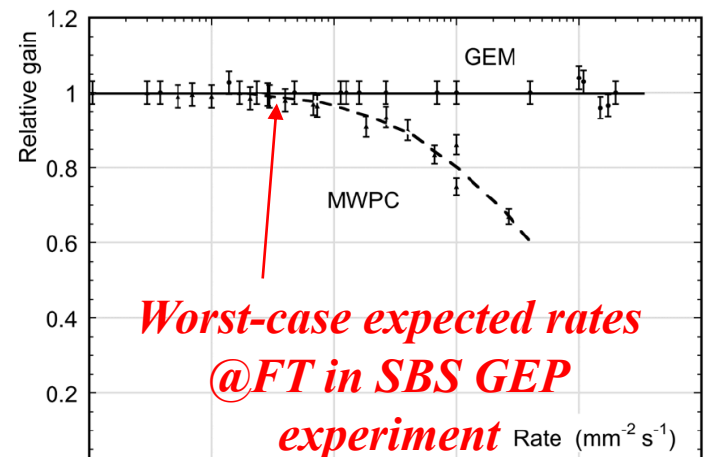
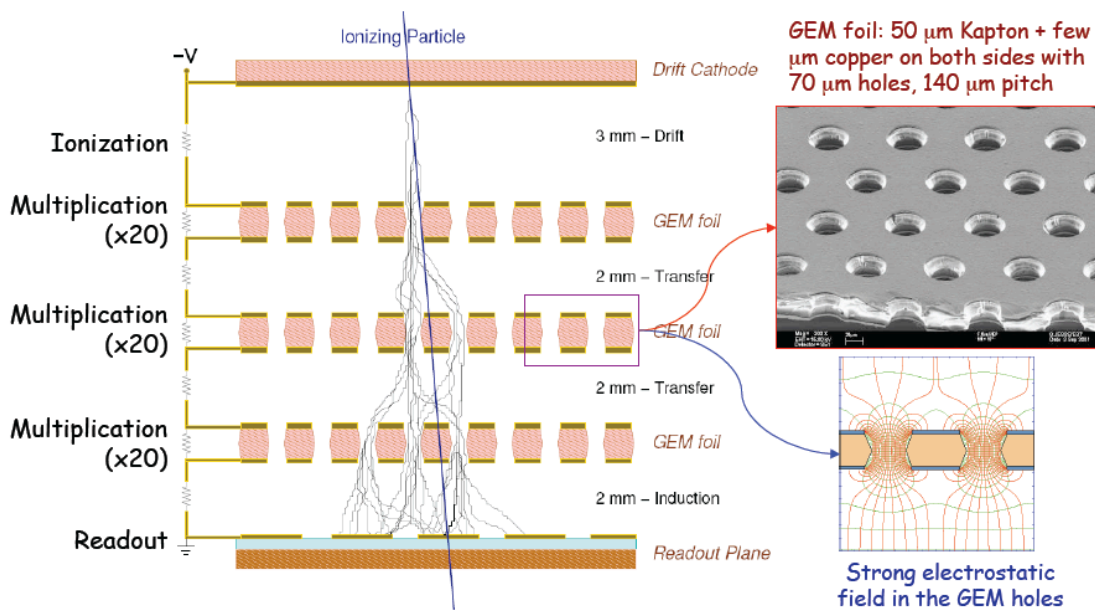
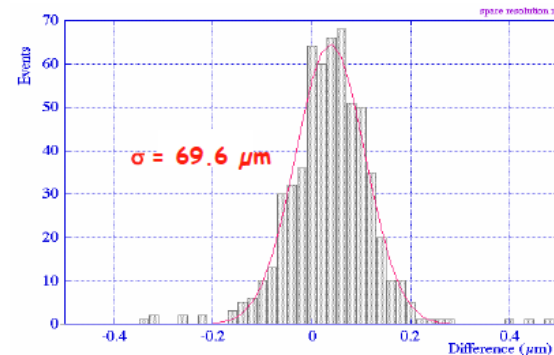


Figure 28.9: Normalized gas gain as a function of particle rate for MWPC [70] and GEM [84].

Stable gain up to very high rates

Recent technology: F. Sauli, NIM A 386, 531 (1997)

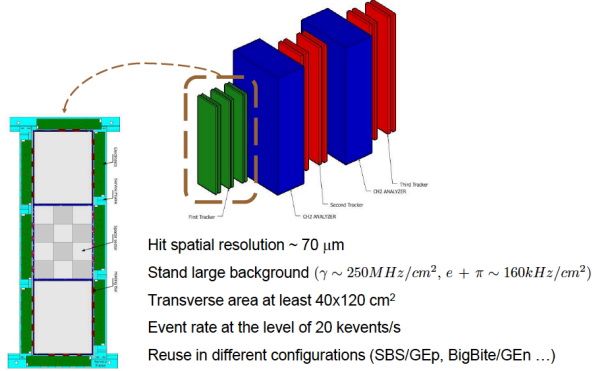
- High spatial granularity
- Ability to cascade several foils: higher gain at lower voltage, reduced discharge risk
- Readout and amplification stages decoupled—XY and/or UV readout strips—pitch 400 μm
- Spatial resolution ~70 μm
- “Fast” signals (for gas ionization detector): intrinsic time resolution <10 ns; arrival time spread ≈ 60 ns for 3-mm gap
- **Enabling technology for SBS physics program! See Kondo Gnanvo talk!**



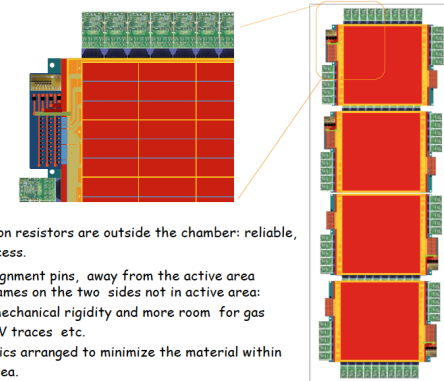
Space resolution

Front Tracker and Polarimeter GEMs (INFN+UVA, others)

SBS trackers/polarimeters:
Front tracker: INFN/UVa



SBS trackers/polarimeters:
Rear tracker: UVa/INFN



GEp/SBS B.Wojtsekhowski

PAC47 July 30, 2019

13

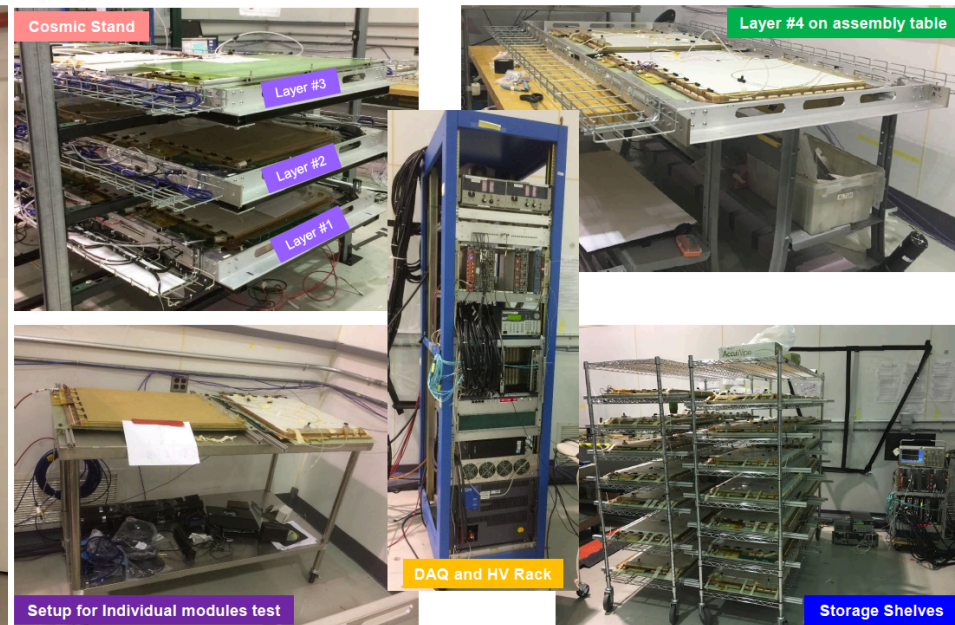
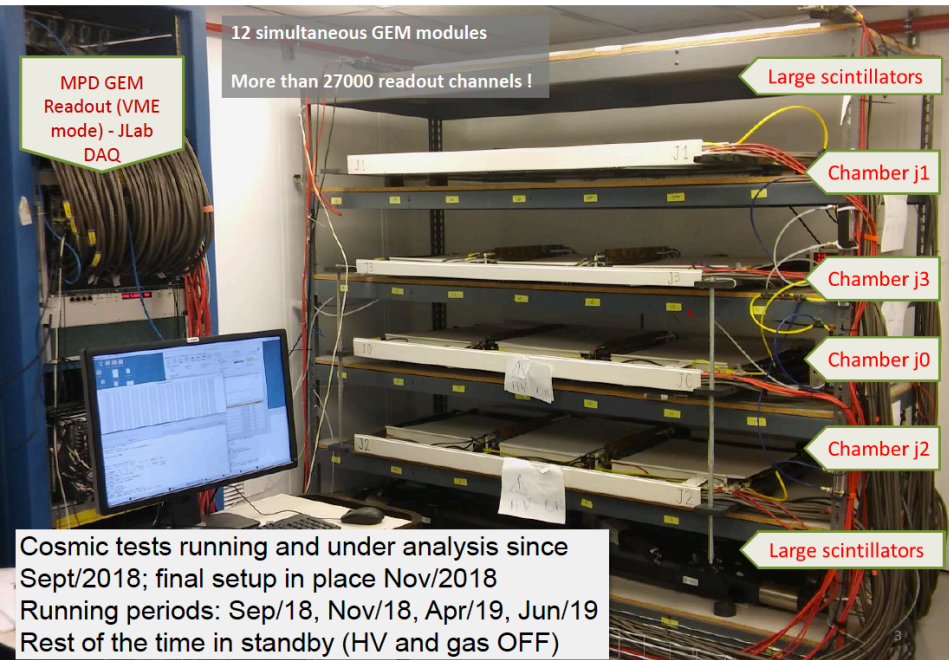
GEM Front Tracker / Cosmic Setup

Nov/18 →



UVa GEMs: Cosmic Setup in EEL124

14



8/6/2019

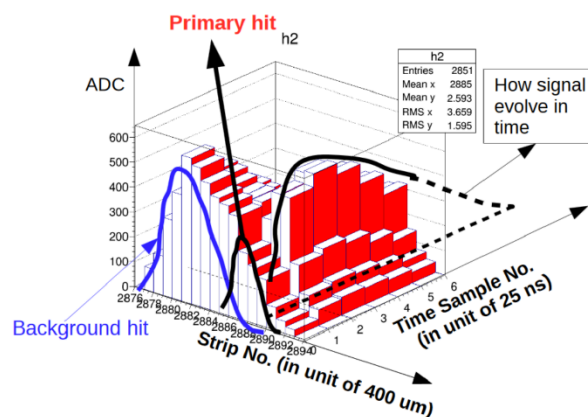
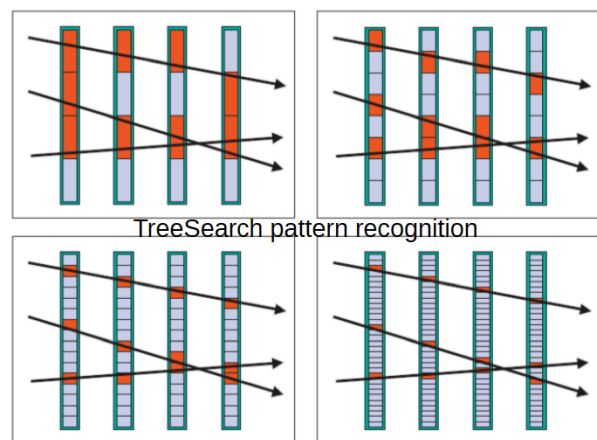
SBS Coll. Meeting @ JLab

6

The tracking challenge at high-luminosity in open geometry: a taste

Reminder: GEM analysis software

- * Primary deployed algorithm using recursive TreeSearch (raw combinatorics also employed for some analyses)
- * GEMs provide six time samples over 25ns bins with jitter
- * Hits are differentiated by fitting to spatial and temporal components
- * Require amplitude matching between x-y components to obtain full 3D reconstruction
- * General restrictions are placed on search areas based on other detector knowledge
- * Basic multithreading implemented



Plot credit :
Danning Di

5

August 6 2019

UConn Jefferson Lab

- In all the SBS experiments, detectors are located in field-free regions behind large dipole magnets with vertical bend*.
- Magnets shield detectors from low-energy *charged* backgrounds, BUT:
- Large flux of low-energy photons into GEMs—can convert in GEMs via Compton/photoelectric effects, pair production.
 - Secondary electrons from soft photon interactions ionize GEM gas, give high rate of background hits: $\sim 0.4 \text{ MHz/cm}^2$ at $Q^2 = 12 \text{ GeV}^2$ in the GEP measurement
- *--except GEP electron calorimeter, which is mainly sensitive to high-energy particles

- High-rate tracking in SBS experiments always relies on external constraints from other detectors, usually total-absorption calorimeters
- Adequate high-rate tracking performance demonstrated for GMN using existing TreeSearch algorithm.
- **However, this approach will not work for GEP, as it relies on analyzing different 2D projections of the track separately.**

UConn Jefferson Lab

1/31/20

Hall A Collaboration Meeting

29

New GEM tracking approach

- To reach high rate, we need to exploit the full dimensionality of the GEM information both at the clustering/hit reconstruction level (x, y, z, t, ADC₁₂₃₄₅₆) and the pattern recognition/track-finding level.
- We must restrict the search region for tracking as much as possible based on information from the other detectors BEFORE we even attempt any clustering or tracking.
- New clustering algorithm is similar to “island” algorithm:
 - Choose one “pixel” (xy strip combination) to seed a cluster based on the largest Pearson correlation coefficient between individual ADC samples on the respective X and Y strips.
 - Build out the cluster from each “seed” pixel by adding nearest neighbor strips meeting certain correlation criteria.
- Do (straight-line) track finding/pattern recognition based on progressive “Kalman Filter-like” approach, implementing constraints from other detectors.
- New tracking code based on this approach successfully tested on (so far) 2018 INFN GEM cosmic ray data and 2016 UVA GEM beam test data from Hall A
- See recent SBS weekly meeting [presentation](#) for more details

$$\rho \equiv \frac{\frac{1}{6} \sum_{i=0}^5 ADCX_i ADCY_i - \mu_x \mu_y}{\sigma_x \sigma_y}$$

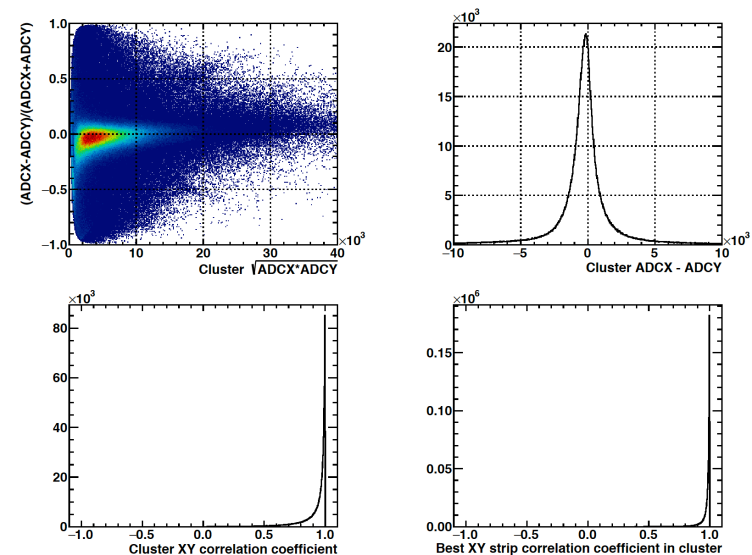
$$\mu_x \equiv \frac{1}{6} \sum_i ADCX_i$$

$$\mu_y \equiv \frac{1}{6} \sum_i ADCY_i$$

$$\sigma_x^2 \equiv \frac{1}{6} \sum_i (ADCX_i)^2 - \mu_x^2$$

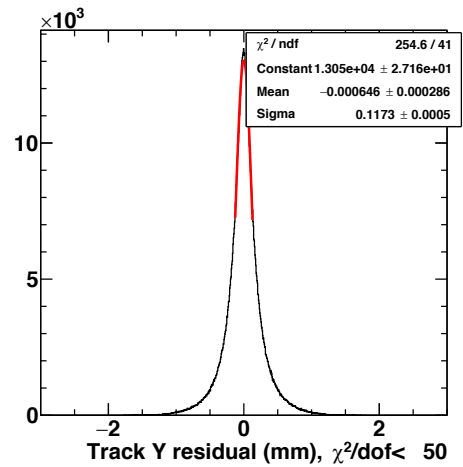
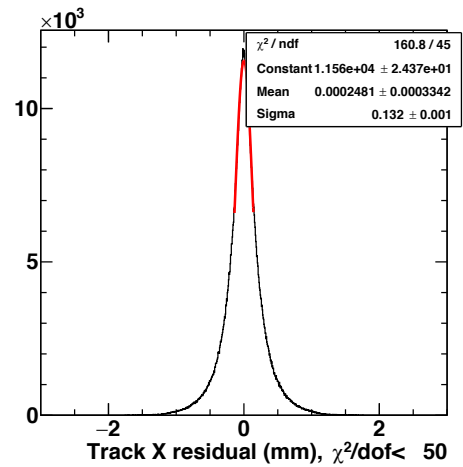
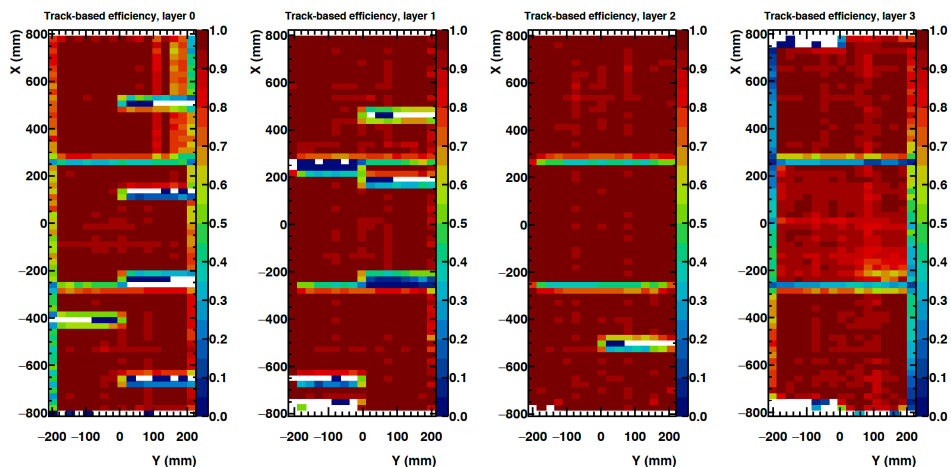
$$\sigma_y^2 \equiv \frac{1}{6} \sum_i (ADCY_i)^2 - \mu_y^2$$

$$-1 \leq \rho \leq 1$$

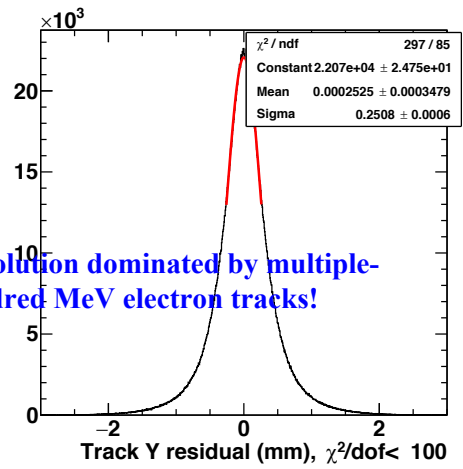
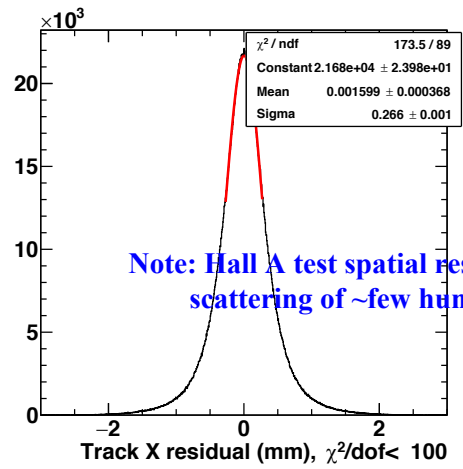
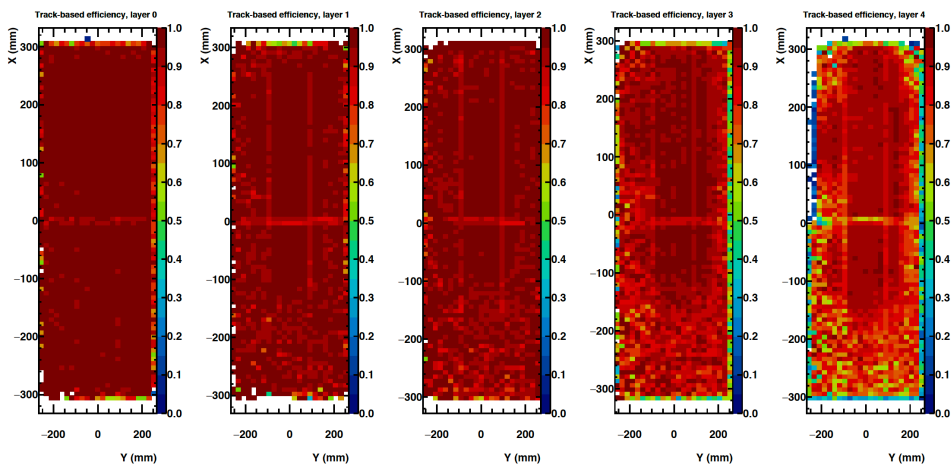


XY correlations from INFN cosmic data

Tracking residuals and track based efficiency



- Above, left: “track based” local GEM efficiency from INFN 4-layer cosmic data, 2018
- Above, right: Tracking residuals from INFN cosmic data: $(\sigma_x, \sigma_y) = (132 \mu m, 117 \mu m)$



Note: Hall A test spatial resolution dominated by multiple-scattering of ~few hundred MeV electron tracks!

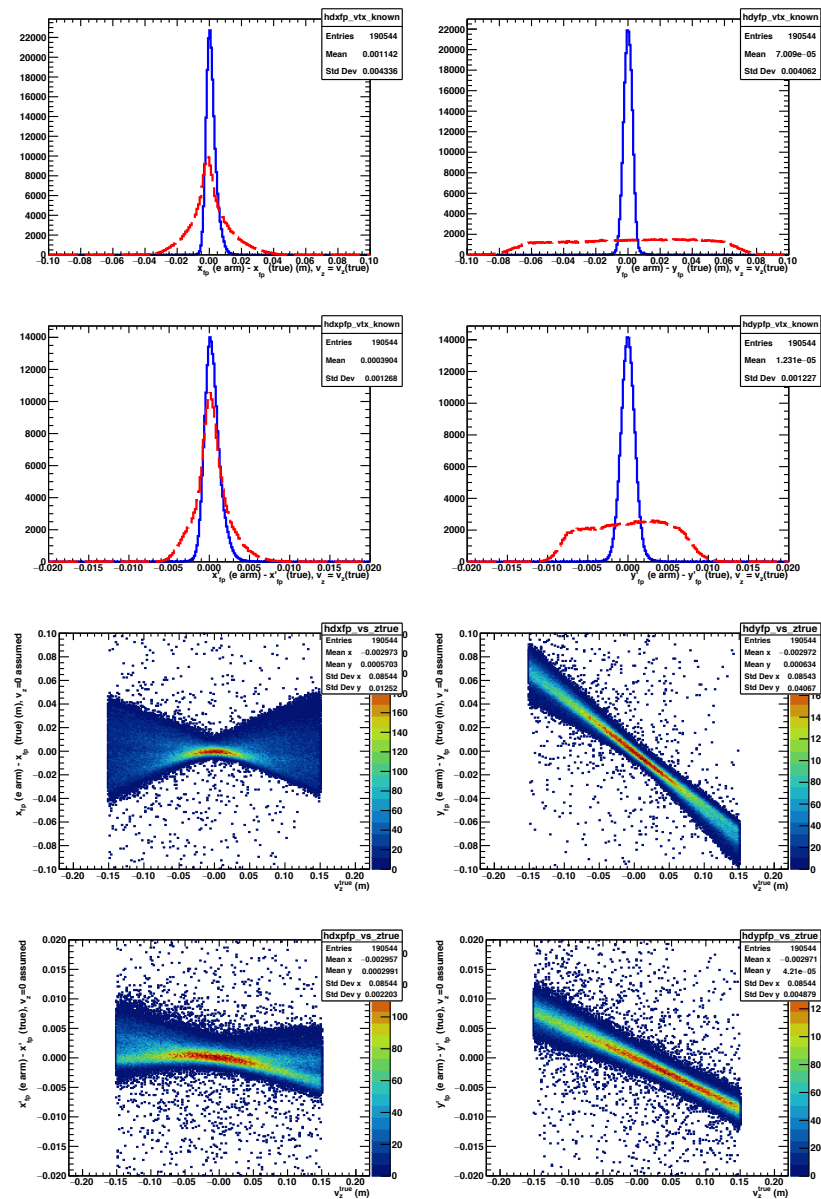
- Above, left: “track based” local GEM efficiency from UVA 5-layer Hall A data, 2016
- Above, right: Tracking residuals from UVA Hall A data: $(\sigma_x, \sigma_y) = (266 \mu m, 251 \mu m)$

Logic of the High-Rate Tracking in GEP

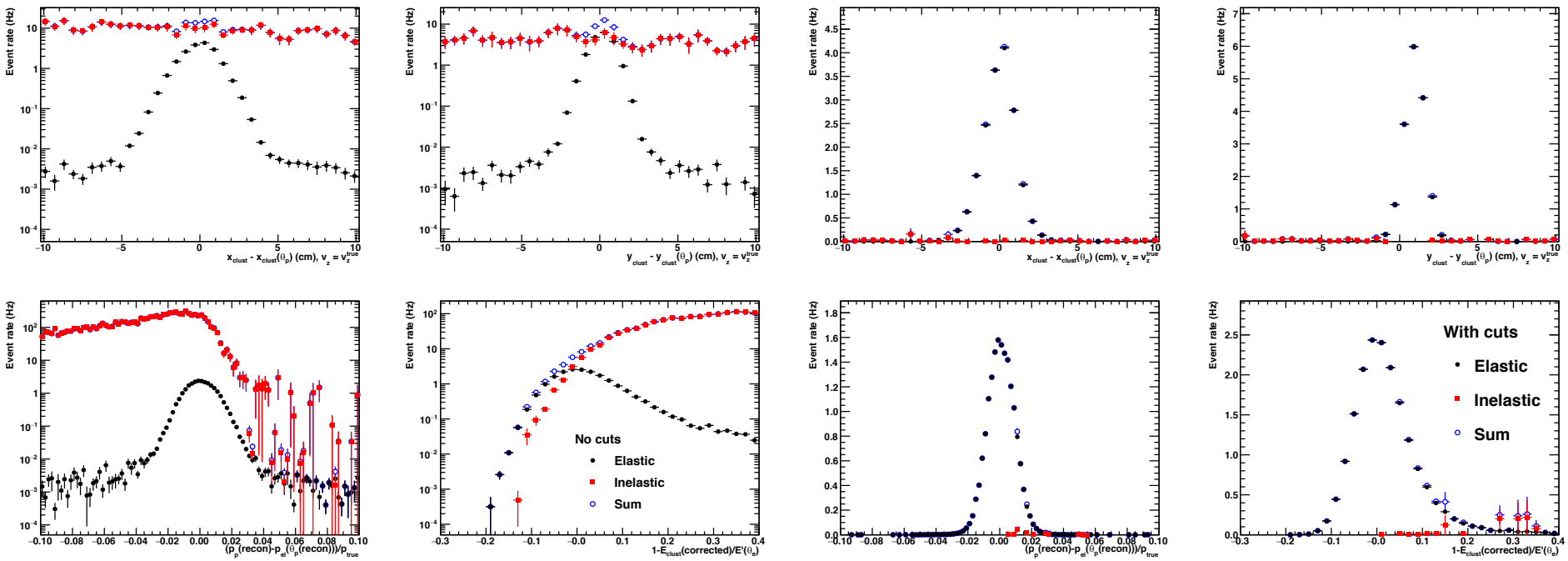
- Random soft photon background hit rate of ~ 400 kHz/cm² leads to high “raw” occupancy of GEM readout strips due to ~ 200 partially overlapping background hits/GEM module/event within 150 ns sampling window
- Six ADC samples/strip at 25 ns/sample, with APV25 pulse shaping electronics:
 - Intrinsic GEM timing resolution < 10 ns
 - Intrinsic GEM spatial resolution ~ 70 μ m
- The charge from primary signal hits is collected in an area of approximately 3 mm² and produces signals on typically 2-4 readout strips in both X and Y (or U and V) directions:
 - Within this 2D area, the probability for a random background hit to overlap with a signal hit within the acquisition window of an event is $\sim 0.2\%$
 - **However, because we have strip readout and not pixel readout, a large fraction of strip signals will be partially contaminated/distorted by background hits in other areas of the GEM \rightarrow biggest challenge in reconstruction!**
 - Severely restrict search area for tracking using electron arm information (FT) and HCAL information (FPP tracker(s))
 - Exploit pulse shape from six-sample readout and XY ADC and timing correlation to suppress background hits
 - Machine learning application?

Exploiting the electron arm information

- Measurement of electron kinematics drastically narrows the allowed search region for proton tracks
- Because our ECAL has no magnets/tracking, it does not constrain the interaction vertex directly.
- Precise vertical coordinate determination with “CDET” constrains azimuthal angle of the reaction plane very well.
- Without knowing the interaction vertex *a priori*, the ECAL+CDET defines an allowed search region at the front tracker of **4 cm (vertical) × 8 cm (horizontal)**, and determines the slope of the proton track to within **±10 mrad** in both directions (minimum horizontal size limited by the 30-cm target thickness)
- If the vertex is known, ECAL+CDET confines the proton track to within a **~1 cm²** area and the direction to within **± 3 mrad** in both directions.
- Tracking strategy involves scanning the assumed vertex location along the target thickness and searching for tracks in a restricted area within each *z* bin consistent with elastic kinematics. Kinematic fitting is also being evaluated to enhance signal/background ratio

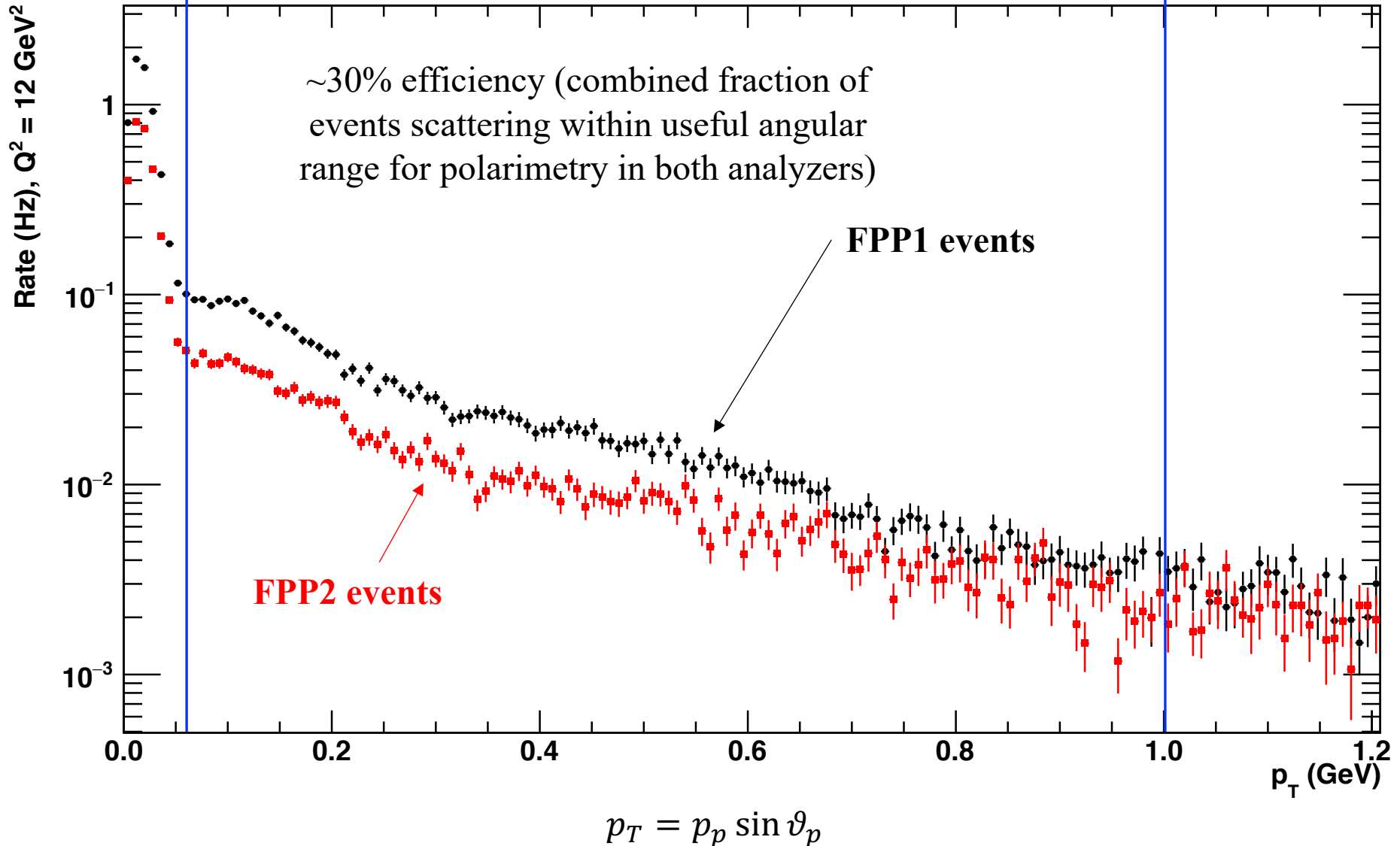


Elastic event selection—Rejecting inelastic backgrounds

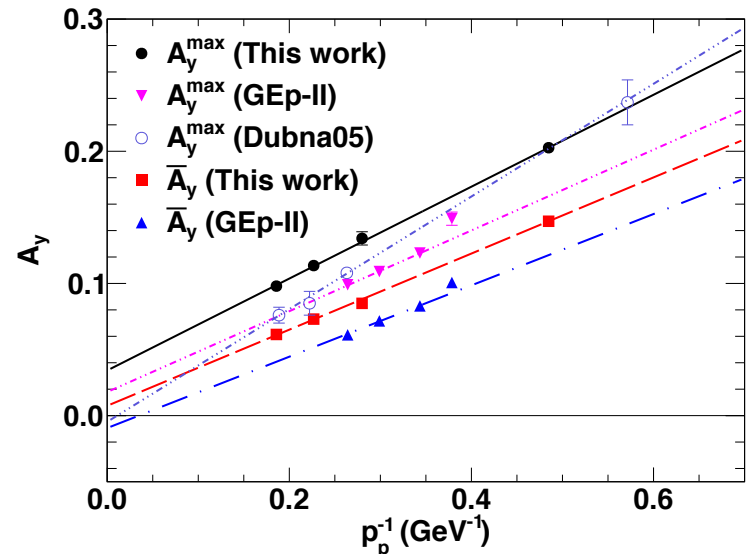
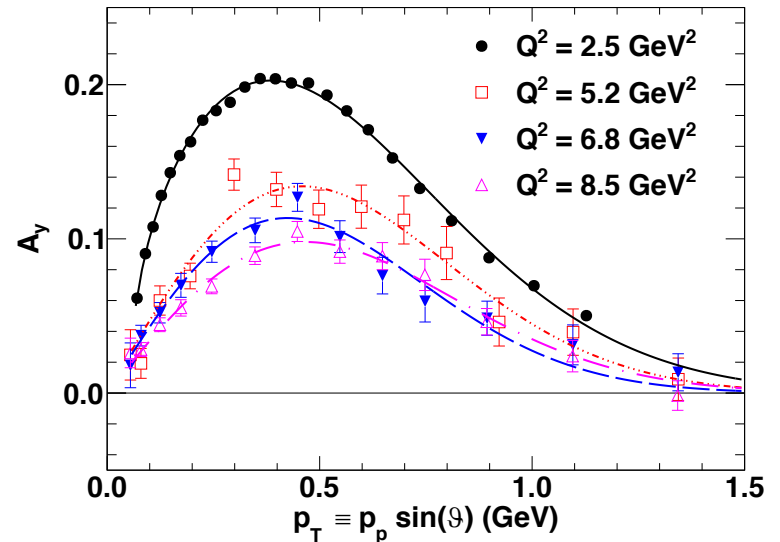
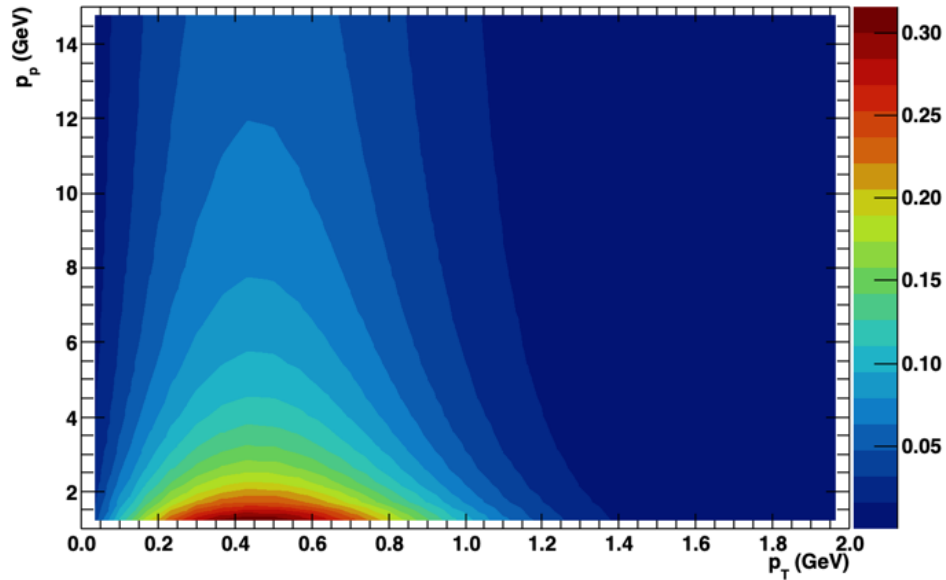


- High rate of inelastic background events will be present in the data, even at high thresholds
- Not many of these inelastic events will actually be reconstructed, since tracking will only even be attempted within a narrow region consistent with elastic kinematics for the detected electron
- Even if these events *were* reconstructed, the combined SBS+ECAL resolution plus exclusivity cuts would suppress inelastic background to <1% (less if kinematic fitting used).

Polarimetry—Efficiency and Angular Distribution



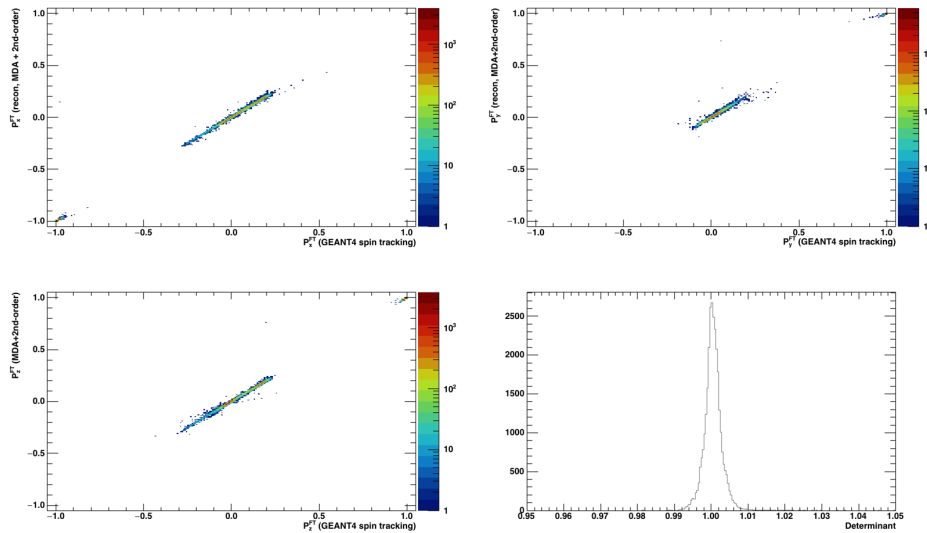
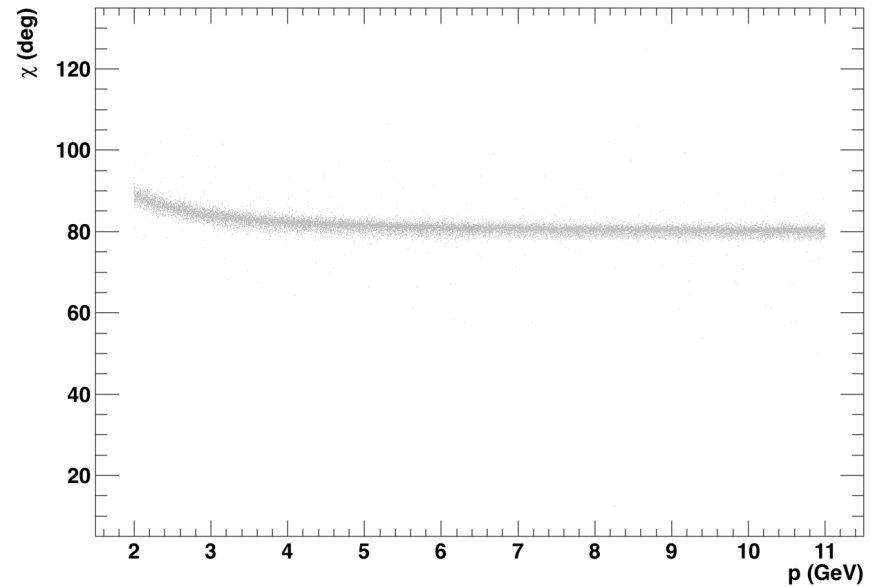
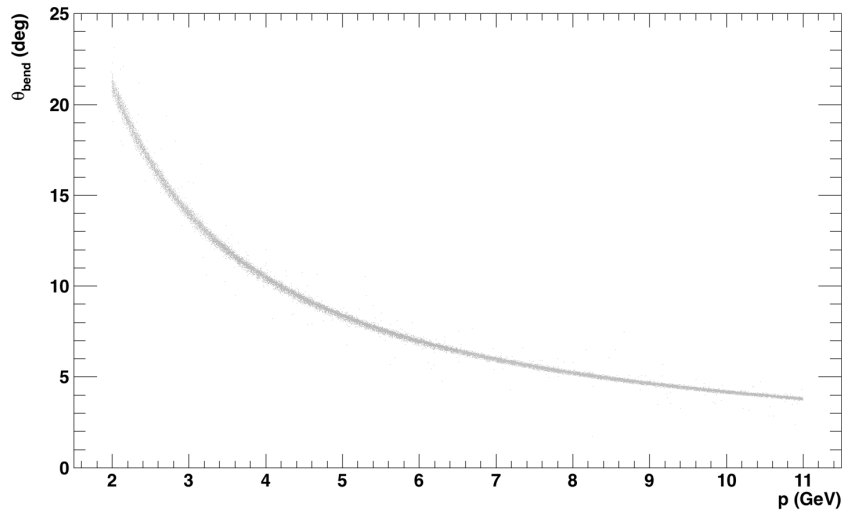
Polarimetry– $p + CH_2$ analyzing power



- From previous experiments, we know that the analyzing power angular distribution has roughly the same shape as a function of $p_T = p_p \sin \vartheta$, with the maximum and average analyzing power decreasing as p_p^{-1} .
- Expected average analyzing power based on modest extrapolation to SBS proton momentum from GEp-III results (shown at right) is $\sim 5.6\%$
- Analyzing power in elastic ep scattering is "self-calibrating"

Polarimetry—Spin Transport

thetabend*57.3:p



- SBS spin transport is much simpler than in previous experiments—simple, non-focusing dipole magnet
- Precession angle $\chi = \gamma\kappa_p\theta_{bend}$ is approximately constant within acceptance
- Fit of full spin tracking to 2nd-order expansion of the deviations from ideal dipole approximation converges—only 15 parameters per rotation matrix element

Polarimetry—Figure-of-Merit Assumptions

- 75 μA beam
- 30 cm LH_2 target
- 85% beam polarization
- SBS dipole field strength scaled with proton momentum
- Analyzing power based on parametrized angular and momentum dependence from GEp-III data (modest extrapolation in momentum)

$$\mathcal{F} \equiv \sum_{i=1}^{N_{event}} (P_e A_y(p_p, p_T))^2$$

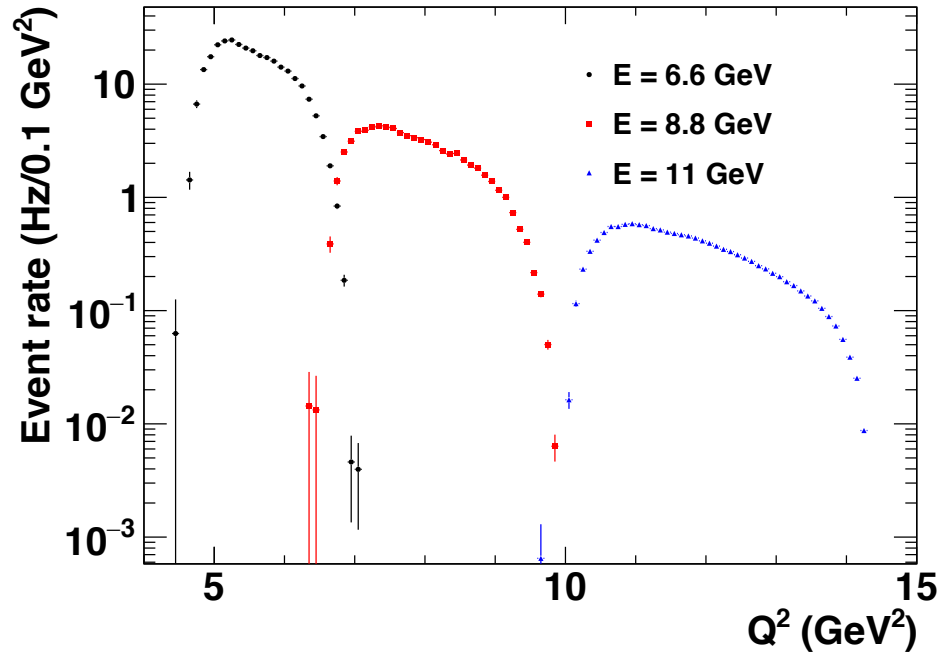
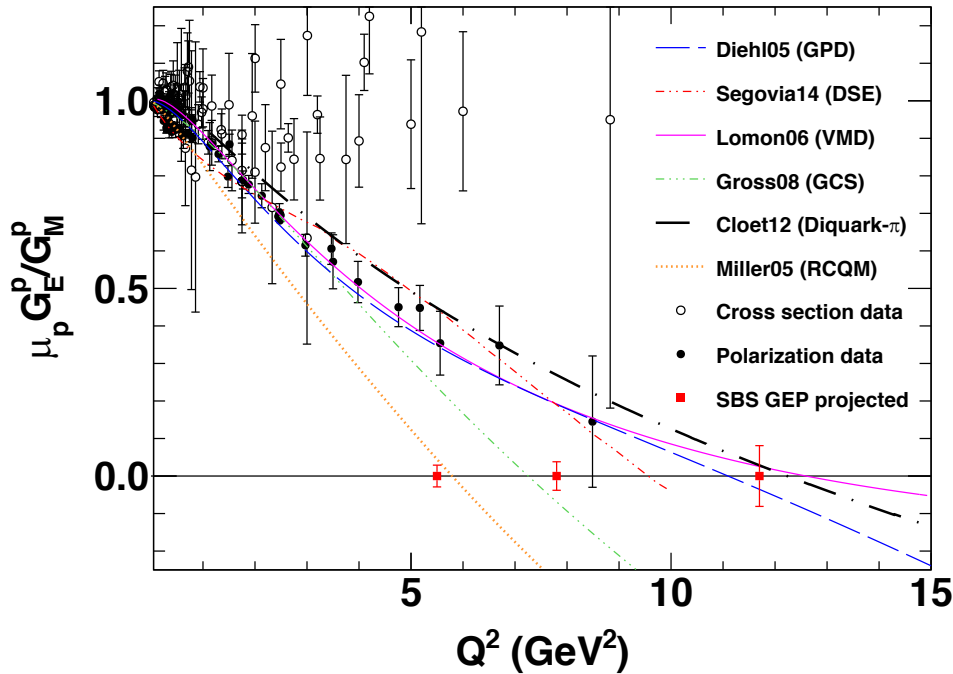
$$\Delta P_{x,y}^{FPP} = \sqrt{\frac{2}{\mathcal{F}}}$$

$$\left(\frac{\Delta R}{R}\right)^2 = \left(\frac{\Delta P_t}{P_t}\right)^2 + \left(\frac{\Delta P_\ell}{P_\ell}\right)^2$$

$$P_t \approx P_x^{FPP}$$

$$P_\ell \approx \frac{P_y^{FPP}}{\sin \chi}$$

SBS G_E^p Projected Results—PAC47 update

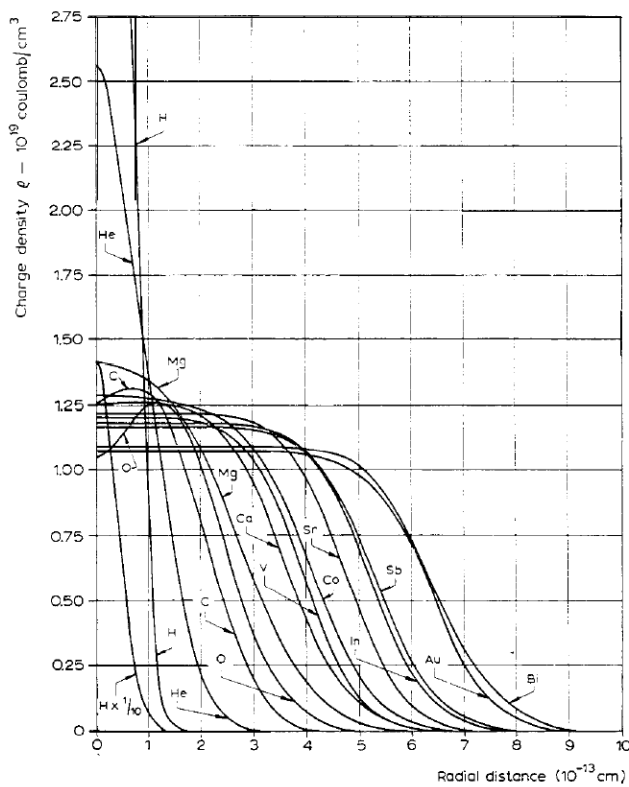


E12-07-109 Jeopardy update re-approved by JLab PAC47, no change in beam time, scientific rating A-

TABLE I. Kinematics, projected accuracy and beam time allocations. The projected statistical uncertainties in the form factor ratio include the assumption of 70% overall event reconstruction efficiency due to the combined efficiencies of the individual detectors, including DAQ dead-time.

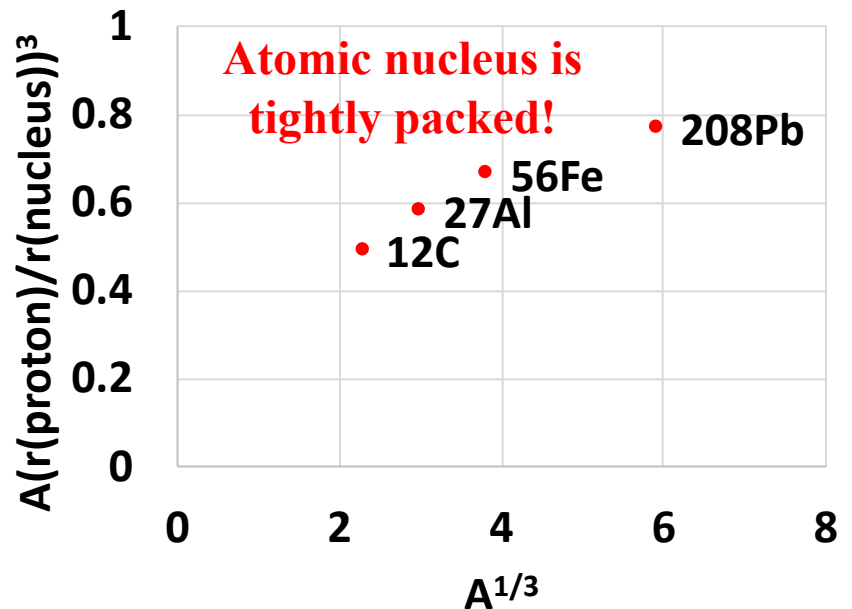
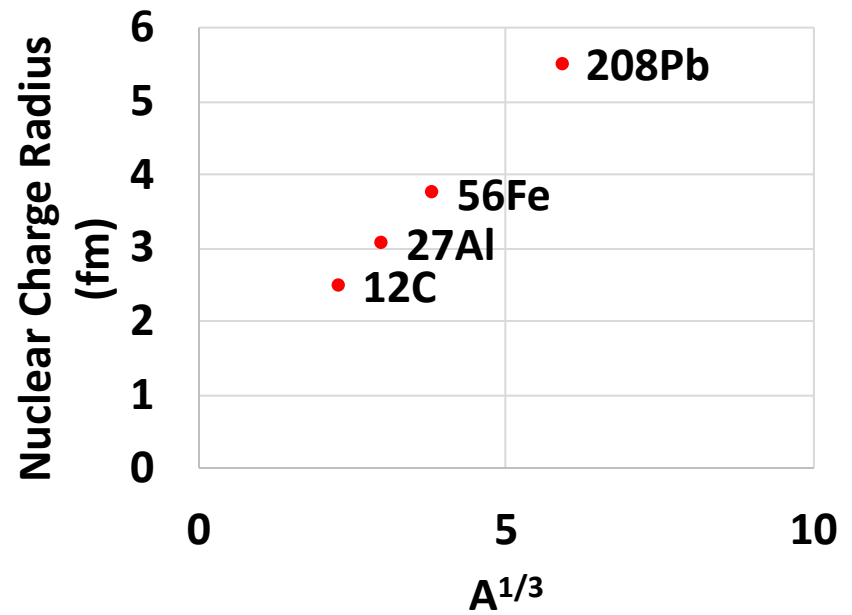
E_{beam} , GeV	Q^2 range, GeV ²	$\langle Q^2 \rangle$, GeV ²	θ_{ECAL} , degrees	$\langle E'_e \rangle$, GeV	θ_{SBS} , degrees	$\langle P_p \rangle$, GeV	$\langle \sin \chi \rangle$, degrees	Event rate, Hz	Days	$\Delta(\mu G_E/G_M)$
6.6	4.5-7.0	5.5	29.0	3.66	25.7	3.77	0.72	291	2	0.029
8.8	6.5-10.0	7.8	26.7	4.64	22.1	5.01	0.84	72	11	0.038
11.0	10.0-14.5	11.7	29.0	4.79	16.9	7.08	0.99	13	32	0.081

Backup



Nuclear Charge Densities

- Above: (R. Hofstadter Nobel lecture): Nuclear charge densities as measured in electron scattering, within Fermi model of the shape
- Top right: example nuclei, $r \sim A^{1/3}$ (volume proportional to number of nucleons)
- Bottom right: “Packing fraction” = ratio of volume of A nucleons to nuclear volume



Nucleon “imaging” (traditional): Rest-frame charge and magnetization densities in 3D space

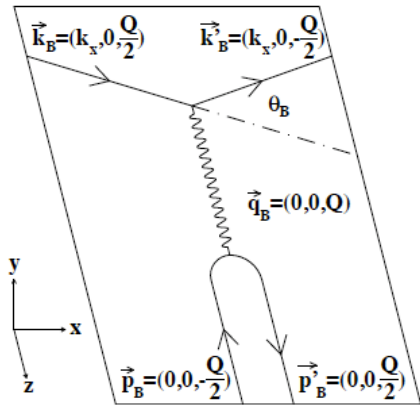


Figure 1-2: Elastic scattering in the Breit frame

$$\lambda_E = \lambda_M = 2$$

$$\tilde{\rho}_{ch}(k) = G_E(Q^2)(1 + \tau)^{\lambda_E},$$

$$\mu \tilde{\rho}_m(k) = G_M(Q^2)(1 + \tau)^{\lambda_M},$$

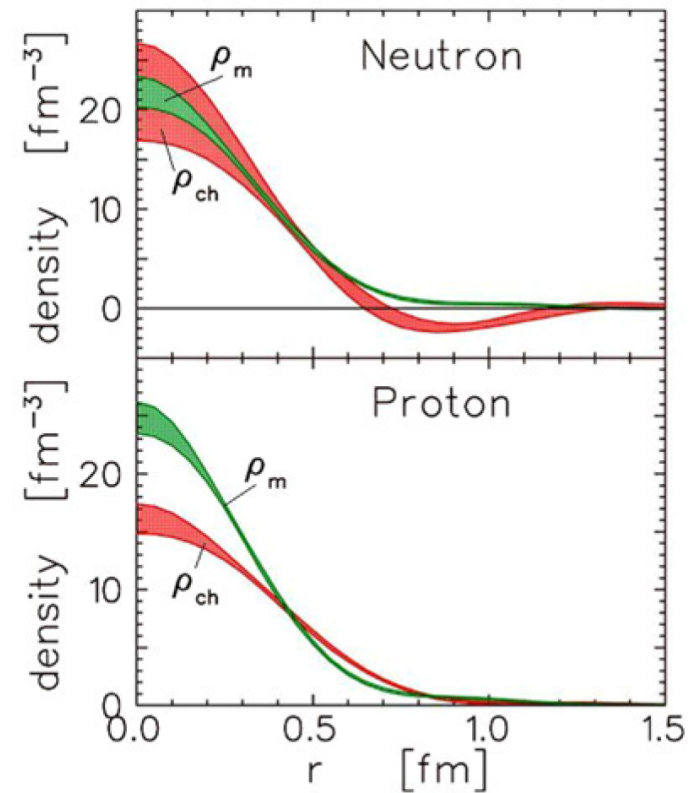
$$\rho(r) = \frac{2}{\pi} \int_0^\infty dk k^2 j_0(kr) \tilde{\rho}(k).$$

$$\tau = \frac{Q^2}{4M^2}$$

$$k^2 = \frac{Q^2}{1 + \tau}$$

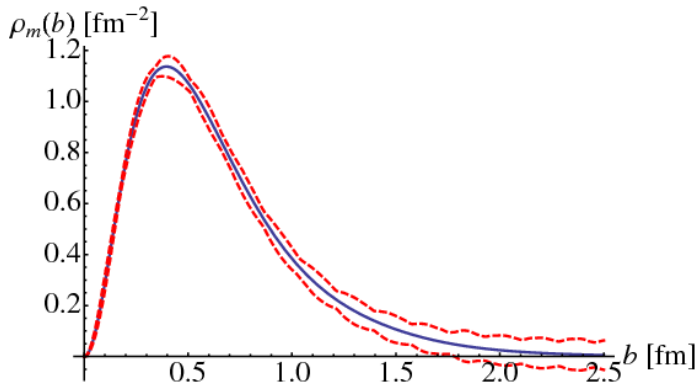
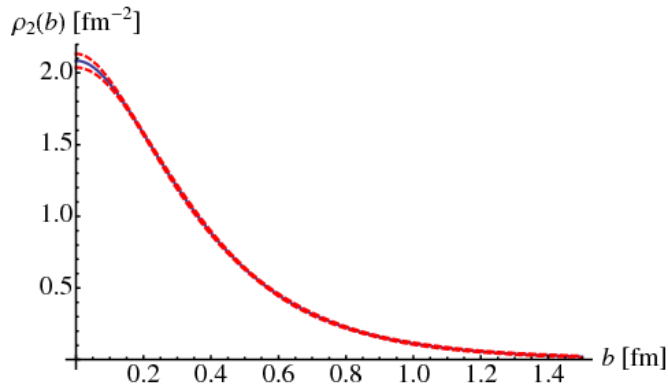
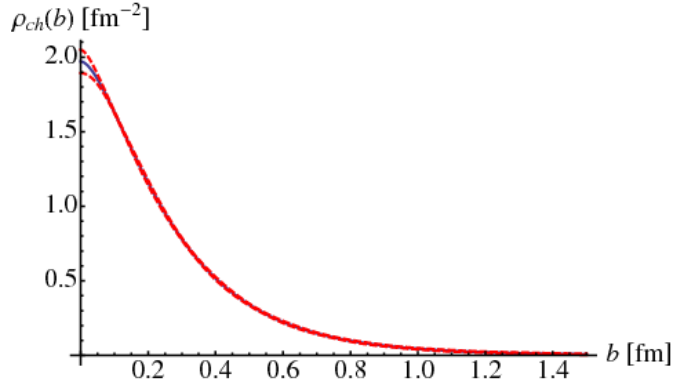
$$\rho_{ch}^{NR}(r) = \frac{2}{\pi} \int_0^\infty dQ Q^2 j_0(Qr) G_E(Q^2),$$

$$\mu \rho_m^{NR}(r) = \frac{2}{\pi} \int_0^\infty dQ Q^2 j_0(Qr) G_M(Q^2),$$



J. J. Kelly: PRC 66, 065203
(2002)

Proton FFs and “imaging”: transverse densities, I



- Miller et al, **Phys. Rev. C, 83, 015203 (2011)**: *model-independent*, impact parameter-space charge and magnetization densities in the infinite momentum frame, derived from GPD-FF sum rules.
- Proton results shown for
 - Charge
 - 2D Fourier transform of F_2 (Pauli FF)
 - Anomalous magnetization density

$$\rho_{ch}(b) = \frac{1}{2\pi} \int Q dQ J_0(Qb) F_1(Q^2)$$

$$\rho_2(b) = \frac{1}{2\pi} \int Q dQ J_0(Qb) F_2(Q^2)$$

$$\rho_m(b) = -b \frac{d}{db} \rho_2(b)$$

$$= \frac{b}{2\pi} \int Q^2 dQ J_1(Qb) F_2(Q^2)$$

Statistical requirements: asymmetries vs. cross section measurements

Cross sections:

$$\sigma \propto N$$

$$\Rightarrow \frac{\Delta\sigma}{\sigma} = \frac{1}{\sqrt{N}}$$

To measure a cross section with a relative statistical precision of 1%, you need 10,000 events.

Asymmetries:

$$\Delta A = \sqrt{\frac{1 - A^2}{N}}$$

$$\frac{\Delta A}{A} = \sqrt{\frac{1 - A^2}{NA^2}}$$

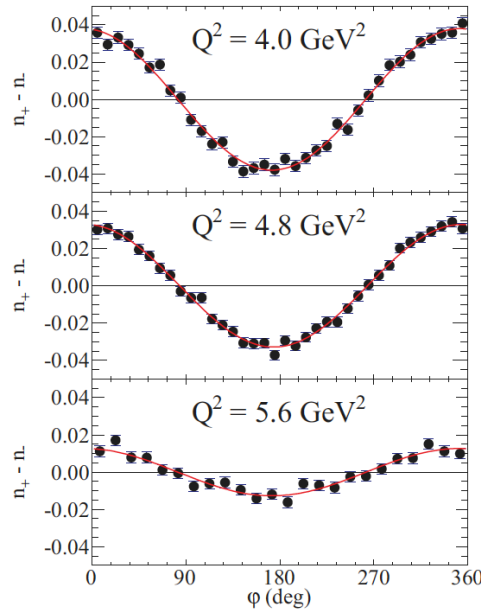


FIG. 6. (Color online) Focal-plane helicity-difference asymmetry $n_+ - n_- \equiv (N_{\text{bins}}/2)[N^+(\varphi)/N_0^+ - N^-(\varphi)/N_0^-]$, where N_{bins} is the number of φ bins and $N^\pm(\varphi)$, N_0^\pm are defined as in Eq. (4), for the three highest Q^2 points from GEp-II. Curves are fits to the data. See text for details.

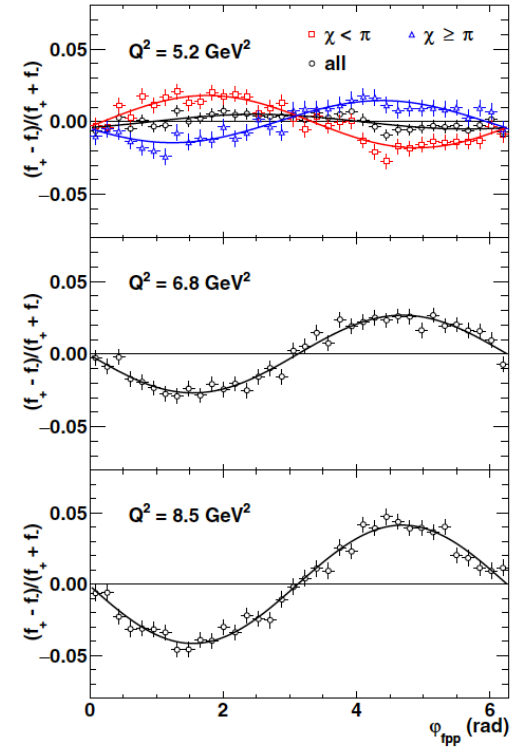


FIG. 10. Focal plane helicity difference/sum ratio asymmetry $(f_+ - f_-)/(f_+ + f_-)$, defined as in Eq. (20), for the GEp-III kinematics, for FPP1 and FPP2 data combined, for single-track events selected according to the criteria discussed in Sec. III B 2. Asymmetry fit results are shown in Table V. The asymmetry at $Q^2 = 5.2 \text{ GeV}^2$ is also shown separately for events with precession angles $\chi < \pi$ and $\chi \geq \pi$, illustrating the expected sign change of the $\sin(\varphi)$ term.

- Typical asymmetry magnitude in a recoil proton polarimeter at "high" momentum is ~few percent.
- For example: to measure a 5% asymmetry with a relative precision of 1%, one needs $N = 10,000 \times \frac{1-A^2}{A^2} \approx 4 \times 10^6$ events!

→ Asymmetry measurement must maximize beam and/or target polarization, and luminosity × acceptance!

FFs and “imaging”: transverse densities, II

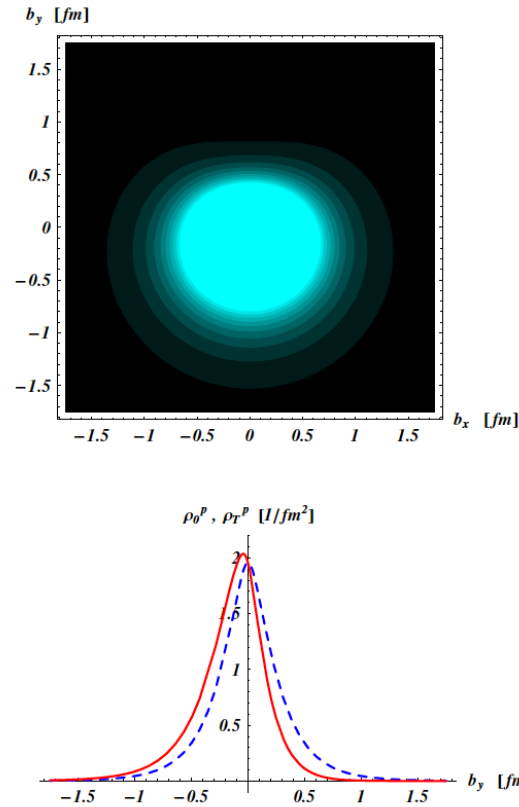


FIG. 1: Quark transverse charge densities in the *proton*. The upper panel shows the density in the transverse plane for a proton polarized along the x -axis. The light (dark) regions correspond with largest (smallest) values of the density. The lower panel compares the density along the y -axis for an unpolarized proton (dashed curve), and for a proton polarized along the x -axis (solid curve). For the proton e.m. FFs, we use the empirical parameterization of Arrington *et al.* [14].

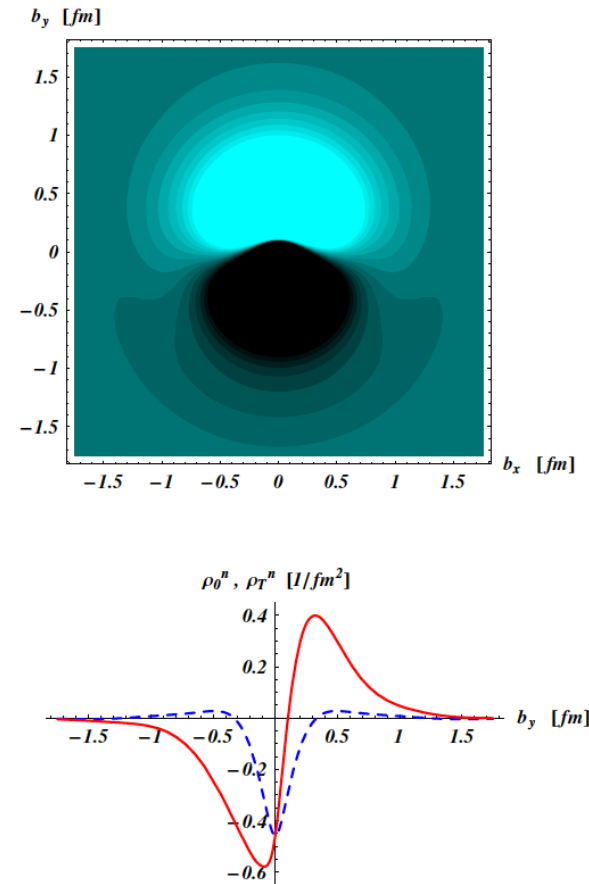


FIG. 2: Same as Fig. 1 for the quark transverse charge densities in the *neutron*. For the neutron e.m. FFs, we use the empirical parameterization of Bradford *et al.* [15].

Proton (left) and neutron (right) 2D polarized transverse charge densities from Carlson and Vanderhaeghen: Phys. Rev. Lett. 100, 032004 (2008)

Simplistic physical picture of form factors—Scattering of ultra-relativistic electrons from a static charge distribution

$$\frac{d\sigma}{d\Omega} = \left(\frac{d\sigma}{d\Omega} \right)_{Mott} |F(\mathbf{q})|^2$$
$$\left(\frac{d\sigma}{d\Omega} \right)_{Mott} \equiv \frac{\alpha^2 (\hbar c)^2}{4E_e^2 \sin^4 \frac{\theta}{2}} \frac{E'_e}{E_e} \cos^2 \frac{\theta}{2}$$
$$F(\mathbf{q}) = \int \rho(\mathbf{x}) e^{i\mathbf{q}\cdot\mathbf{x}} d^3x$$

- In the one-photon-exchange approximation in QED (equivalent to the first Born approximation in nonrelativistic quantum scattering theory), the cross section factorizes as the product of the “Mott” cross section, and the square of the *form factor* $F(\mathbf{q})$, equal to the Fourier transform of the charge density with respect to the three-momentum transfer $\mathbf{q} = \mathbf{k} - \mathbf{k}'$
- The Mott cross section represents the theoretical cross section for scattering of ultrarelativistic, spin-1/2 electrons from a point-like, spin-less target of charge e .
- In the non-relativistic limit, $Q^2 \ll M^2$, we have the correspondence: $|F(\vec{q})| = G_E(Q^2)$

Form Factors for a point nucleon

$$\begin{aligned}
 G_E^p(Q^2 = 0) &= 1 \\
 G_M^p(Q^2 = 0) &= \mu_p = +2.793 \\
 G_E^n(Q^2 = 0) &= 0 \\
 G_M^n(Q^2 = 0) &= \mu_n = -1.913 \\
 F_1^p(0) &= 1 \\
 F_2^p(0) &= \kappa_p = \mu_p - 1 = +1.793 \\
 F_1^n(0) &= 0 \\
 F_2^n(0) &= \kappa_n = -1.913
 \end{aligned}$$

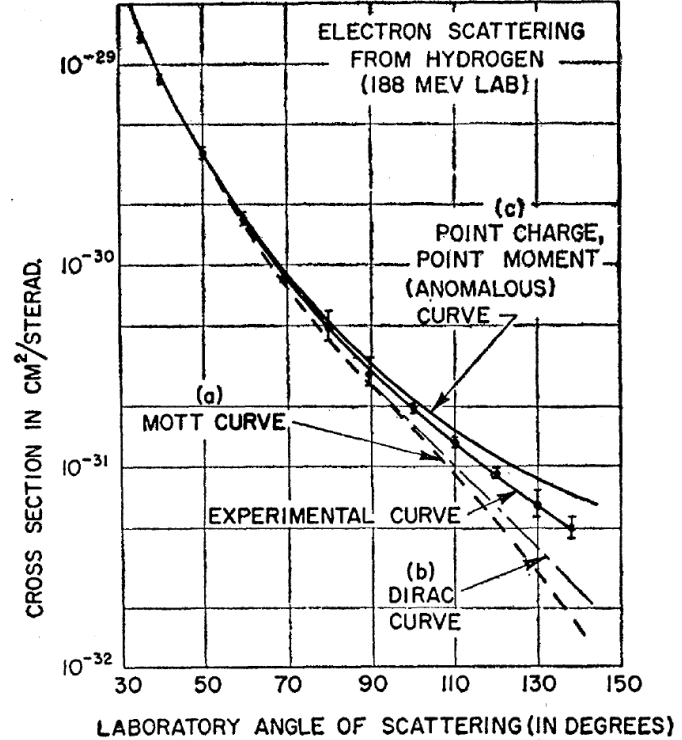


FIG. 24. Electron scattering from the proton at an incident energy of 188 Mev. The experimental points lie below the point-charge point-moment curve of Rosenbluth, indicating finite size effects.

R. Hofstadter, Rev. Mod. Phys., 28, 214 (1956)

- In the low- Q^2 (long-wavelength) limit, the electric and magnetic form factors reduce to the proton and neutron charges and magnetic moments.
- If the nucleon were pointlike, the form factors would have these constant values at any Q^2

R. Hofstadter

Nobel Prize 1961



"for his pioneering studies of electron scattering in atomic nuclei and for his thereby achieved discoveries concerning the structure of the nucleons"

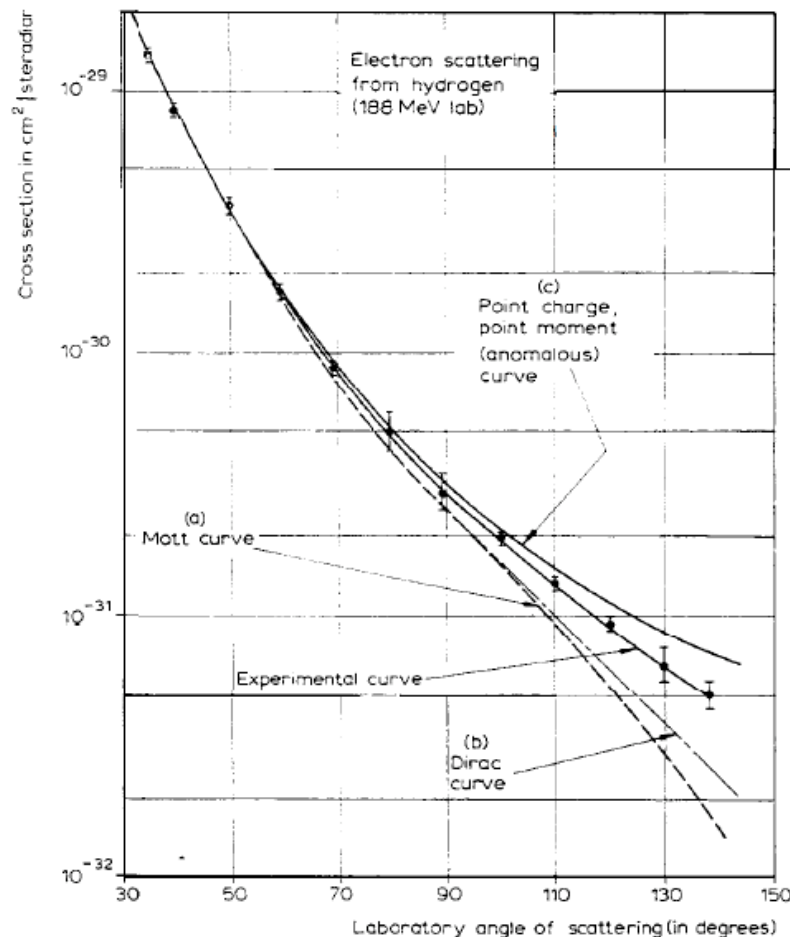


Fig. 9. Electron scattering from the proton at an incident energy of 188 MeV. Curve (a) shows the theoretical Mott curve for a spinless point proton. Curve (b) shows the theoretical curve for a point proton with a Dirac magnetic moment alone. Curve (c) shows the theoretical behavior of a point proton having the anomalous Pauli contribution in addition to the Dirac value of the magnetic moment. The deviation of the experimental curve from the Curve (c) represents the effect of form factors for the proton and indicates structure within the proton. The best fit in this figure indicates an rms radius close to $0.7 \cdot 10^{-13}$ cm.

Measuring Form Factors—Rosenbluth Separation

- The nucleon structure-dependent part of the cross section factorizes from the “point-like” part.
- The “reduced cross section” σ_R depends linearly on ϵ for a given Q^2 , with slope G_E^2 and intercept τG_M^2 .
- Experimentally, one measures $d\sigma/d\Omega$ while varying the beam energy and scattering angle to change ϵ while holding Q^2 constant

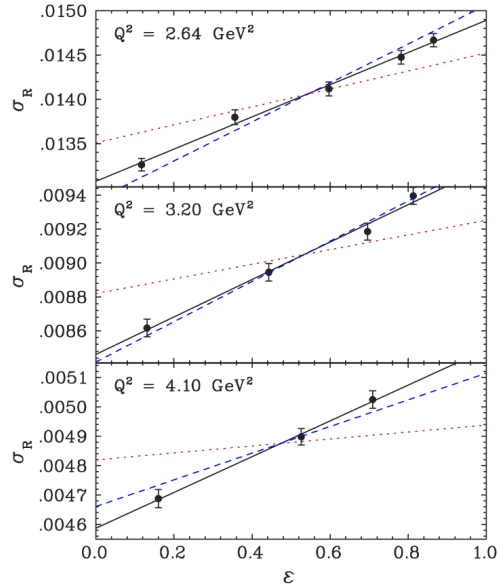


FIG. 2 (color online). Reduced cross sections as a function of ϵ . The solid line is a linear fit to the reduced cross sections, the dashed line shows the slope expected from scaling ($\mu_p G_E/G_M = 1$), and the dotted line shows the slope predicted by the polarization transfer experiments [6].

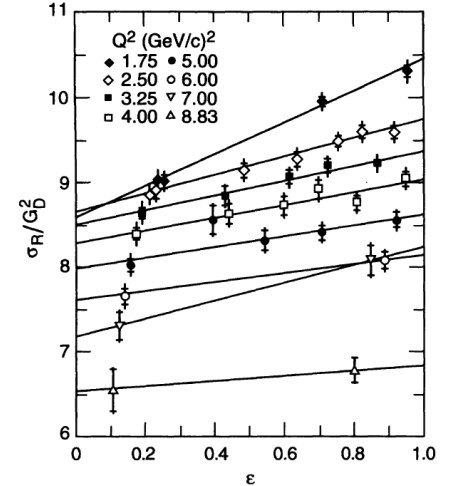


FIG. 22. Reduced cross sections divided by the square of the dipole fit plotted versus ϵ for each value of Q^2 . The 1.6 GeV data points correspond to the leftmost point on each line, and the E136 data point is the rightmost point on the $Q^2 = 8.83$ (GeV/c) 2 line. The inner error bars show the statistical error, while the outer error bars show the total statistical and point-to-point systematic errors. An overall normalization uncertainty of $\pm 1.77\%$ has not been included.

Qattan *et al.*, **Phys. Rev. Lett.** 94, 142301 (2005)

Andivahis *et al.*, **Phys. Rev. D** 50, 5491 (1994)

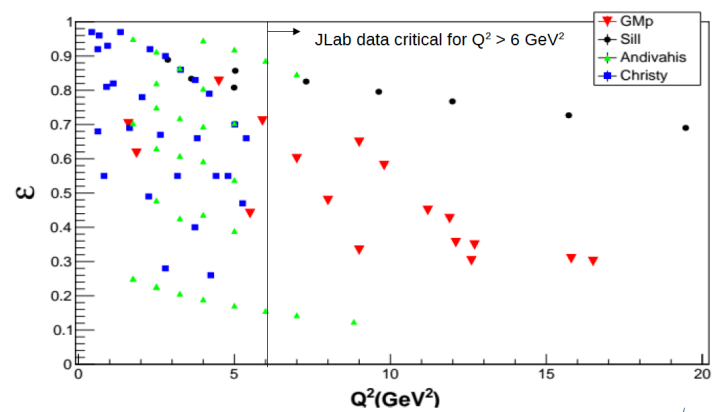
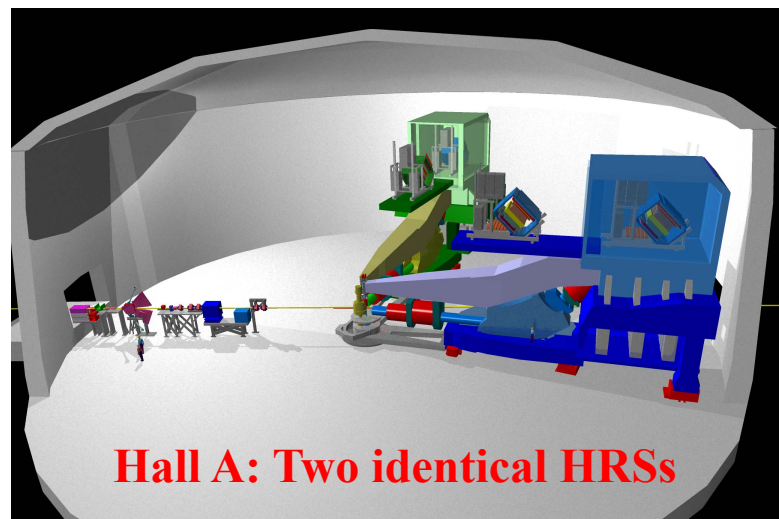
$$\frac{d\sigma}{d\Omega_e} = \left(\frac{d\sigma}{d\Omega_e} \right)_{Mott} \frac{\epsilon G_E^2 + \tau G_M^2}{\epsilon(1 + \tau)}$$

$$\left(\frac{d\sigma}{d\Omega_e} \right)_{Mott} = \frac{\alpha^2 \cos^2 \left(\frac{\theta_e}{2} \right) E'_e}{4E_e^2 \sin^4 \left(\frac{\theta_e}{2} \right) E_e}$$

$$\sigma_R = \epsilon G_E^2 + \tau G_M^2$$

$$\tau \equiv \frac{Q^2}{4M_p^2}$$

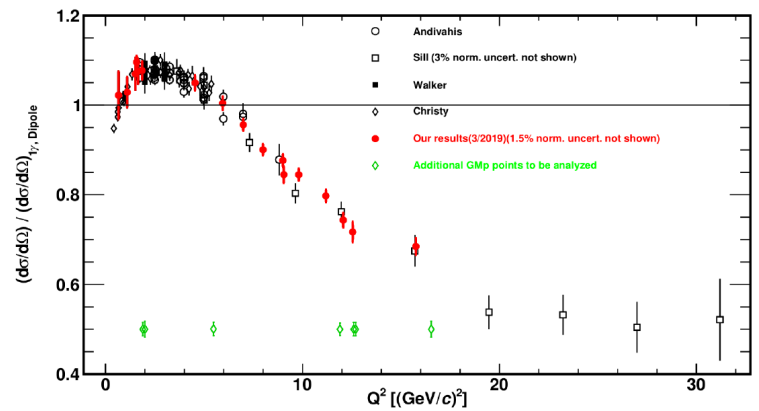
$$\epsilon \equiv \left[1 + 2(1 + \tau) \tan^2 \left(\frac{\theta_e}{2} \right) \right]^{-1}$$



- GMP12 data at much smaller ϵ than Sill data
- Less sensitivity to G_E in extracting G_M
- Lever arm in ϵ provides sensitivity to:
 - 2γ from global fit utilizing G_E / G_M from polarization transfer

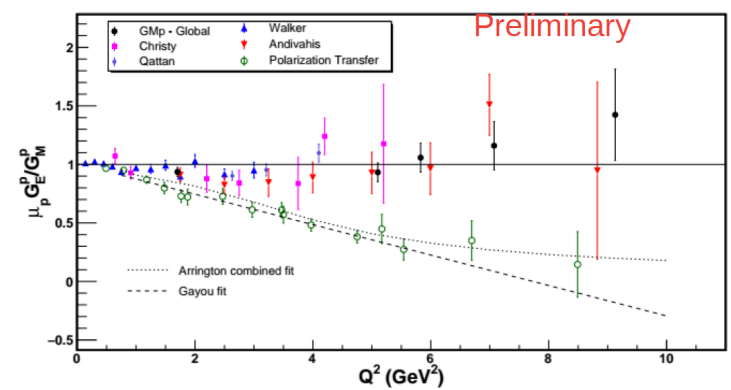
$$\frac{d\sigma}{d\Omega} = \sigma_{Mott} \frac{\epsilon (G_E^p)^2 + \tau (G_M^p)^2}{\epsilon (1 + \tau)}$$

GMP - E012-07-108 final cross sections



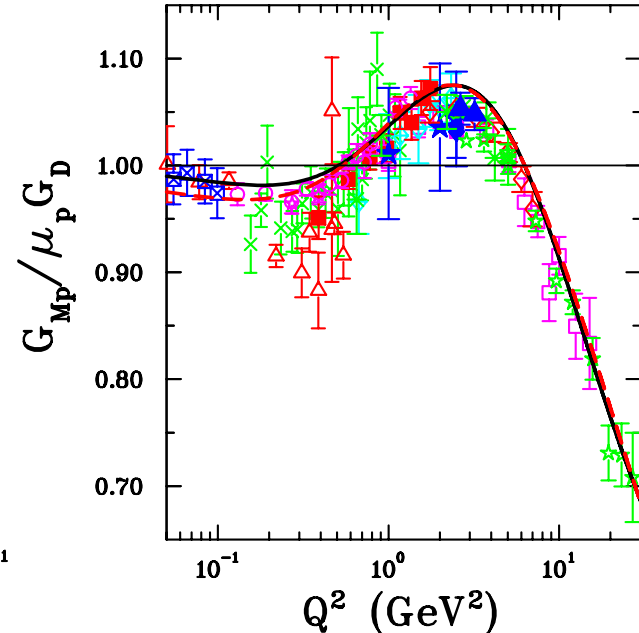
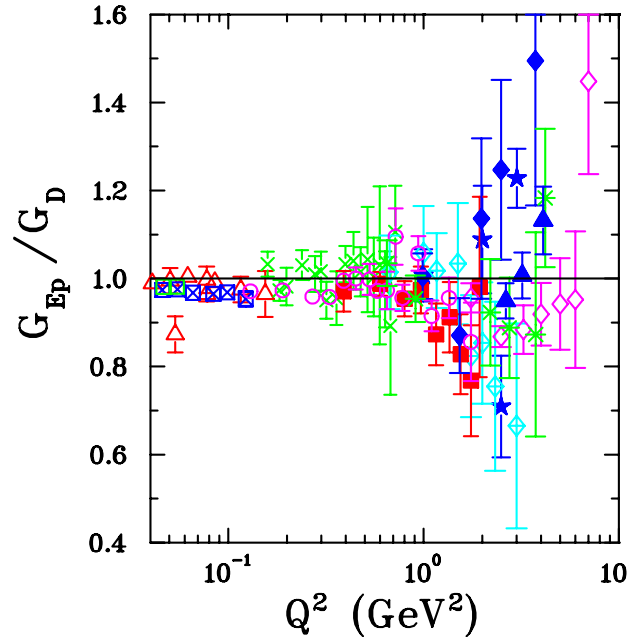
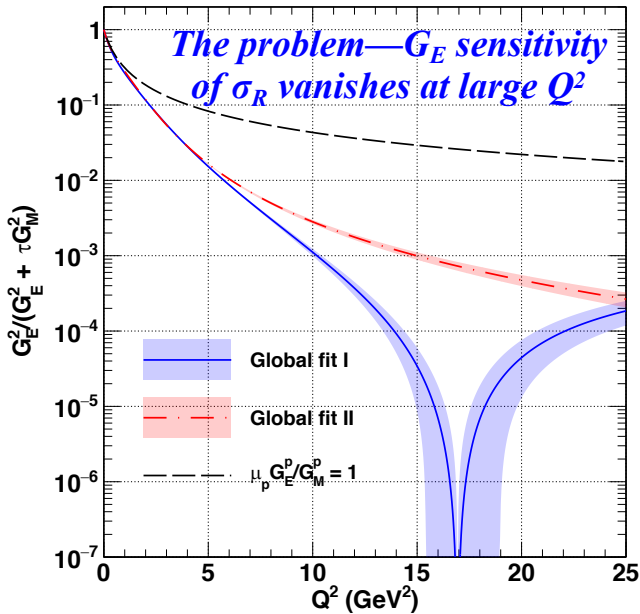
- Cross section relative to 1- γ cross section calculated with $G_E = G_M / \mu = G_{dip}$
 - Significant improvement in precision for $Q^2 > 6$.
 - Systematic uncertainties on Fall 2016 LHRS data $\sim 1.3\%$ (pt-pt), 1.5% (norm)
- RHRS (additional 2% from optics)

Impact of E12-07-108 data on G_E / G_M at large Q^2



- Lab Hall A GMP12 data significantly reduce uncertainties on G_E / G_M at largest Q^2 => further highlights discrepancy with P-T data up to $Q^2 > 9$
- Full data set provides significantly more sensitivity than shown in select L/T separations

Proton FFs—Rosenbluth data



Maximum contribution of G_E^2 term to σ_R vanishes at large τ .
Fits to FF data are described in

[Phys. Rev. C, 96, 055203 \(2017\)](#)

$$\sigma_R = \epsilon G_E^2 + \tau G_M^2$$

G_E^p and G_M^p Rosenbluth Data: $G_E^p \approx \frac{G_M^p}{\mu_p} \approx G_D$

$$G_D \equiv \left(1 + \frac{Q^2}{\Lambda^2}\right)^{-2}$$

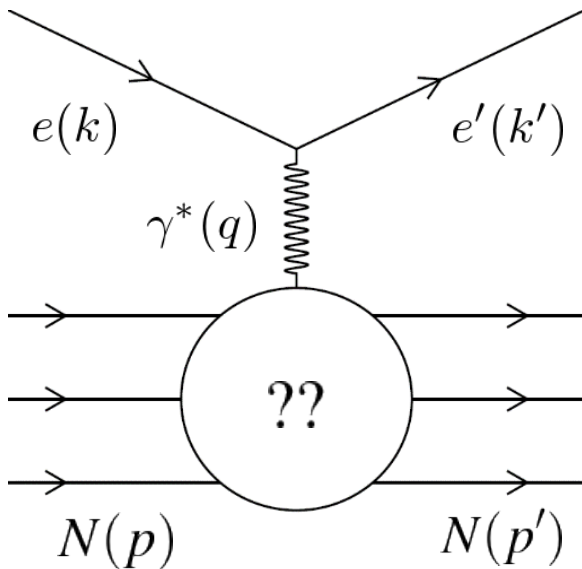
$$\Lambda^2 = 0.71 \text{ GeV}^2$$

- Elastic ep cross sections have been measured for $0.003 \leq Q^2 \leq 31.2 \text{ GeV}^2$.
- Rosenbluth data for G_E^p and G_M^p are qualitatively described by the “dipole” form factor, which is the Fourier transform of a spherically symmetric, exponentially decreasing radial charge/magnetization density.

Elastic eN scattering and form factors: formalism

$$\mathcal{M} = \frac{4\pi\alpha}{q^2} \bar{u}(k') \gamma^\mu u(k) g_{\mu\nu} \bar{u}(p') \left[F_1(q^2) \gamma^\nu + F_2(q^2) \frac{i\sigma^{\nu\alpha} q_\alpha}{2M} \right] u(p)$$

Invariant amplitude for elastic eN scattering in the one-photon-exchange approximation



- The most general possible form of the virtual photon-nucleon vertex consistent with Lorentz invariance, parity conservation and gauge invariance is described by two form factors F_1 (Dirac) and F_2 (Pauli):
 - F_1 describes the helicity-conserving amplitude (charge and Dirac magnetic moment)
 - F_2 describes the helicity-flip amplitude (anomalous magnetic moment contribution)

$$G_E \equiv F_1 - \tau F_2$$

$$G_M \equiv F_1 + F_2$$

$$\tau \equiv \frac{Q^2}{4M^2}$$

Sachs Form Factors G_E (electric) and G_M (magnetic), are experimentally convenient linearly independent combinations of F_1, F_2

$$\sigma_R \equiv \frac{\epsilon(1 + \tau) \left(\frac{d\sigma}{d\Omega_e} \right)}{\left(\frac{d\sigma}{d\Omega_e} \right)_{Mott}} = \epsilon G_E^2 + \tau G_M^2$$

$$\frac{d\sigma}{d\Omega_e} = \frac{\alpha^2 (\hbar c)^2 \cos^2 \frac{\theta_e}{2}}{4E_e^2 \sin^4 \frac{\theta_e}{2}} \frac{E'_e}{E_e} \left[\frac{\epsilon G_E^2 + \tau G_M^2}{\epsilon(1 + \tau)} \right]$$

$$\frac{1}{\epsilon} \equiv 1 + 2(1 + \tau) \tan^2 \frac{\theta_e}{2}$$

Differential cross section in the nucleon rest frame:

Rosenbluth formula

Rosenbluth Separation Method: Measure cross section at fixed Q^2 as a function of ϵ to obtain G_E^2 (slope) and G_M^2 (intercept).